National Library of Canada

Acquisitions and Bibliographic Services Branch

395 Wellington Street
Ottawa, Ontario
K1A 0N4

Bibliothèque nationale du Canada

Direction des acquisitions et des services bibliographiques

395, rue Wellington
Ottawa (Ontario)
K1A 0N4

Your file Votre référence

Our file Notre référence

NOTICE

The quality of this microform is heavily dependent upon the quality of the original thesis submitted for microfilming. Every effort has been made to ensure the highest quality of reproduction possible.

If pages are missing, contact the university which granted the degree.

Some pages may have indistinct print especially if the original pages were typed with a poor typewriter ribbon or if the university sent us an inferior photocopy.

AVIS

La qualité de cette microforme dépend grandement de la qualité de la thèse soumise au microfilmage. Nous avons tout fait pour assurer une qualité supérieure de reproduction.

S'il manque des pages, veuillez communiquer avec l'université qui a conféré le grade.

La qualité d'impression de certaines pages peut laisser à désirer, surtout si les pages originales ont été dactylographiées à l'aide d'un ruban usé ou si l'université nous a fait parvenir une photocopie de qualité inférieure.

Canada

Pressure Induced Phase Transitions in CuO and Cu_2O

by

Richard Legault

Thesis submitted to the University of Ottawa
in partial fulfillment of the requirements
for the degree of Master of Science

Department of Physics
University of Ottawa

ISBN 0-612-04878-0

Canada

UNIVERSITÉ D'OTTAWA
UNIVERSITY OF OTTAWA

Abstract

We have studied samples of CuO and Cu_2O to pressures of 60 GPa and 35 GPa, respectively, using energy dispersive X-ray diffraction. Samples were studied using a gasketed diamond anvil cell, energy dispersive X-ray diffraction at the Cornell High Energy Synchrotron Source, with a Mo or $Al_2O_3:Cr^{3+}$ pressure gauge. In the case of Cu_2O, the two phase transitions, (cubic to hexagonal to another hexagonal) as expected were seen. In CuO no definite phase transition was seen, although indications are given for CuO at 60 GPa converting to a distorted rocksalt-type structure from the initial monoclinic structure. The volume data obtained from the pressure experiments on CuO were best fitted with the third-order Birch-Murnaghan equation of state with B_0=110 GPa and B_0'=5.5.

Statement of Originality

The following observations appear to be original:

a) A sample of CuO was studied to a pressure of 60 GPa using X-ray diffraction with synchrotron radiation, surpassing the previous record of 50 GPa.

b) Indications for a phase transition in CuO from the monoclinic structure to a distorted rocksalt-type structure near 60 GPa.

c) A chemical reaction between the pressure medium, methanol:ethanol, and a sample of CuO leading to the formation of Cu.

d) Cu_2O was studied to 35 GPa using X-ray diffraction with synchrotron radiation, surpassing the previous record of 24 GPa.

Acknowledgments

I would like to thank the students, faculty and staff at the University of Ottawa Physics Department. They have made the last two and a half years quite enjoyable. In particular, I would like to thank, Mike Jackson, Mike Murphy, Dave LeBlanc, Rob Parent, Laura Sears, and Loraine Gravelle.

Outside the department I would like thank my friend Cindy Rathje, my parents, Ron and Pat and my brother, David. They have always encouraged me to continue my studies and have only asked that I do my best.

I would like to thank Ken Lagarec, for without his brilliance in the programming of the XRDA program, I would still be analyzing spectrums. I would like to thank Ken for his discussions and insight into the behaviour of structures under pressure.

Finally I would like to thank my supervisor, Serge Desgreniers. The least of his accomplishments was the arduous task of reading my many revisions of this thesis, for that I am grateful. His insight and our debates and discussions have paved the way for this thesis.

Table of Contents

List of Tables and Figures

Page

Page

§1 Introduction

To properly fulfill the requirements of this research project, a variety of topics had to be thoroughly investigated. A diverse list of subjects and topics that benefit from or lend themselves to the high pressure research field are briefly introduced and discussed. This leads to a brief discussion of the techniques and apparati used to generate high pressure and to probe a sample under high pressure. In section 1.2, the possible benefits of high pressure research on the samples of CuO and Cu_2O are discussed. In addition to the benefits of high pressure research, the current state of research on these oxides is also mentioned.

Once the pressure is generated and the necessary data is obtained, the next step is to develop a model to explain the behaviour of the sample. The models used for the two types of high pressure research, static and dynamic, are derived and their uses are discussed.

To end the chapter, an in-depth examination of the various monoxides is accomplished. To help in the analysis of the data, the concept of the packing fraction is introduced and explained. Finally the phases of CuO and Cu_2O previously reported are described.

§1.1 The High Pressure Research Field

Over the last century many techniques have been used to investigate the effects of pressure on materials. One of these methods involved the firing of a high velocity projectile at a slab of material under investigation. This method is commonly referred to as dynamic pressure measurements. An earlier method involved the use of presses and anvils to generate high pressures. This method has evolved into the diamond anvil cells (DAC) that are commonly used today in high pressure physics. The measurements attained through the use of these devices are categorized as static pressure measurements.

The early anvils were produced from hardened steel and were thus opaque to visible light and X-rays. In order to study the effects of pressure in such a DAC, the electrical resistivity of the sample was measured, indicating what the changes in the band gap were occurring. For instance, solid xenon's band gap of 9 eV at room pressure, gradually decreases to 4 eV at 60 GPa.[1] This change in the band gap is due to a rearrangement of atomic positions inside the lattice resulting in electron band overlap and thus an altering of the materials resisitivity. Along with resistivity other techniques including X-ray diffraction, Mössbauer, Raman and Brillouin spectroscopy are being used to study phase transitions in samples.

The change of physical properties of a sample is due to the contraction of the lattice as the pressure is increased. Any measurements made on the sample will change smoothly in response to this gradual change of the relative atomic positions. At a certain pressure, a phase change may occur if the new lattice structure is energetically more favourable in comparison to the previous structure. Such a change in structure results in a dramatic change in atomic positions, resulting in a discontinuity in the resistivity, or other physical measurements taken. In the case of X-ray diffraction or Raman spectroscopy, the discontinuity most likely results in the absence of former peaks and the occurrence of new ones.

In some cases the change can be visibly detected due to a change of the material band gap. Along with this visible change, the resistivity of the sample may change from that of an insulator to a conductor. Such a transition for example has been observed in samarium monosulfide. SmS transforms from a dull black semiconductor, at room pressure, to a gold coloured conductor at 0.7 GPa.[2] Another example, where pressure induces a change of a physical property is found in the field of superconductor research: the critical temperature of La_2CuO_4 has been shown to rise from 37.6 K at room pressure to 42.4 K at 1.9 GPa.[3]

For reference, the pressure at which SmS transforms, namely 0.7 GPa, is nearly equivalent to 7000 atmospheres. The most popular and efficient device used to attain and surpass such immense pressures is the diamond anvil cell (DAC). The DAC works on the principle that high pressure is attained from the application of force over a small area. Thus the amount of sample placed in the pressure chamber between the diamond anvils must necessarily be small, of the order 10^{-12} m^3. A major obstacle to static high pressure experiments is to design probes that do not require large amounts of sample to achieve a respectable signal and give reliable physical data about the material under pressure.

Since this research project is concerned with the behaviour of CuO and Cu_2O lattice structures under pressure, a natural choice for this investigation would be X-ray diffraction. To achieve a diffraction spectrum from this small amount of material, placed inside the DAC, would require hundreds of hours of beam time from a standard copper tube X-ray diffractometer. Fortunately, today's synchrotron source will yield a large enough luminosity, due to the high velocity of the electrons, to allow an X-ray diffraction pattern to be recorded in a reasonable amount of time. At the Cornell High Energy Synchrotron Source (CHESS), where most of the data presented in this work have been obtained, a "good" diffraction spectrum of material CuO required only 1-2 hours of beam time. For these reasons X-ray

diffraction by synchrotron radiation was used for the investigations on the behaviour of CuO and Cu_2O under pressure.

§1.2 Reasons for High Pressure Studies on CuO and Cu_2O

A valid response by many scientists to the question of why should a research project be undertaken, is similar to that of the mountain climber Sir Edmund Hillary, because it (Mt. Everest) is there. In other words the main justification for research on any sample is simple curiosity. We may have ulterior motives for the study of CuO and Cu_2O but the true reason is simply to discover how it will react under pressure. Will it behave as predicted? Will a phase transition at some pressure not yet attained, occur? Will it yield some yet unknown characteristic due to the pressure increase? These are all questions for which answers can be found through this and other research projects. There is also the possibility that the research itself will present new questions about the behaviour of the sample under pressure. To answer these new questions, different methods of analyzing the data may be sought or new experiments that may yield answers to these questions may be devised.

One of the questions that this research hopes to shed light on is: Is there some sort of relationship between similar oxide compounds in relation to there behaviour under pressure? This question will be discussed.

The study of CuO may lead to predictions of which phase transitions will occur in AgO or other monoclinic structures. Likewise the investigation of Cu_2O could lead to similar predictions for Ag_2O or other cubic structures. It should be mentioned that the Ag compounds have not been studied as extensively as the Cu compounds. These studies may also lead towards a method of predicting the behaviour of complex compounds that contain a significant amount of copper and oxygen in their composition as is the case for some high-T_c superconductors. In particular, how the bond between Cu-O affects the physical characteristics of the sample.[4]

§1.3 Equations of State for Solids

To allow researchers to properly interpret their data and be able to compare results with one another, a series of equations of state have been developed. Equation of state (EOS) can be derived empirically or from basic physical principles to explain the change in volume with pressure. Thus far, there are only two classes of EOS derived from basic physical principles, one for dynamic results (to be discussed later) and another set for static measurements.

We shall briefly review these two models.

1.3.1 Modeling of the Isothermal Equations of State

A well developed equation of state accurately predicts what the volume is at any given pressure, barring a phase change. In developing an EOS the following questions are asked:

What causes the volume to change in this way?
Why does a material that is malleable at low pressure become harder to compress as the pressure increases?
Can we mathematically mimic this behaviour?

Equations of state come in various forms, the simplest being the one defined by the thermodynamics of an ideal gas:

$$PV = nRT \qquad (1.1).$$

This equation was developed under the premise that the material consists of non-interacting particles. This premise is not valid for a solid since by definition a solid does consist of interacting particles.

Another simple EOS, is one that considers the meaning behind the bulk modulus B of a material:

$$B = -\frac{dP}{d\ \ln V} = \frac{dP}{d\ \ln \rho} \qquad (1.2).$$

For this case, the EOS is obtained by integration of (1.2) to yield:

$$V = V_0 \exp\left(\frac{-P}{B_0}\right) \qquad (1.3),$$

but this is only valid for pressures near room pressure where the value for the bulk modulus, B_0, is measured. Recall that a material becomes less compressible at higher pressures therefore the bulk modulus must change with pressure.

Murnaghan demonstrated[5] that the local bulk modulus could be modeled by:

$$B=\frac{1}{3}(3\lambda+2\mu+P_0) \qquad (1.4),$$

where the constants λ and μ, are dependent on the initial pressure P_0. If λ and μ are linear functions of P_0 then the bulk modulus B is also a linear function of P_0:

$$B=B_0+kP_0 \qquad (1.5)$$

and with equation (1.3):

$$d\ln\rho=\frac{d\,P}{B_0+kP_0} \qquad (1.6),$$

$$P(\rho)=\frac{B_0}{k}\left[\left(\frac{\rho}{\rho_0}\right)^k-1\right] \qquad (1.7),$$

where k could be replaced by $B_0'=(d\,B/d\,P)_{P=0}$. Equation (1.7) is used to describe the EOS of materials and is referred to as the *Murnaghan integrated linear EOS* or simply the *Murnaghan EOS.*

For the Murnaghan EOS, equation (1.7), one notes that the finite strain on the internal lattice was not taken into account. The Birch-Murnaghan EOS[6] was developed to take the finite strain into account:

$$9B_{0T}V_0=\lim_{P\to 0}\left(\frac{1}{f}\,\frac{\partial F}{\partial f}\right)_T \qquad (1.8),$$

where F is the free energy of the lattice and is expanded in terms of the compression f:

$$F=a(T)f^2+b(T)f^3+c(T)f^4+... \qquad (1.9).$$

If F is expanded to second order then:

$$F=a(T)f^2$$

and results in the *Second-Order Birch-Murnaghan EOS*:

$$P(V)=\frac{3B_0}{2}\left[\left(\frac{V}{V_0}\right)^{-\frac{7}{3}}-\left(\frac{V}{V_0}\right)^{-\frac{5}{3}}\right] \qquad (1.10).$$

A further expansion of equation (1.9) leads to the *Third-Order Birch-Murnaghan EOS*:[6]

$$P=\frac{3}{2}B_0\left[\left(\frac{V}{V_0}\right)^{-\frac{7}{3}}-\left(\frac{V}{V_0}\right)^{-\frac{5}{3}}\right]\left[1+\frac{3}{4}(B_0'-4)\left\{\left(\frac{V}{V_0}\right)^{-\frac{2}{3}}-1\right\}\right] \qquad (1.11).$$

The EOS parameters, B_0 (the atmospheric bulk modulus at room pressure) and B_0' (the change in the bulk modulus with pressure at room pressure), are found by using a non-linear least squares or χ^2-minimization routine to fit the experimental data to the chosen EOS model.

1.3.2 Modeling of the Hugoniot: The Equations of State for Shock Compressed Matter.

In order to accomplish static pressure measurements, a technique is required to measure the pressure at which the sample is placed. The best method for measuring the pressure on a sample, is to place a pressure gauge inside the DAC along with the sample. Unfortunately there is no convenient absolute pressure gauge available, that can be placed inside the DAC. Thus it is necessary to create a secondary pressure gauge by calibrating it with a primary pressure gauge. So how do we calibrate this secondary pressure gauge to high pressure without extrapolation? Fortunately, just after the end of the Second World War, the military laboratories initiated a series of dynamic high pressure research programs to study materials under high compression. As will be discussed later, data obtained by dynamic measurements could be analyzed to yield results that are equivalent to static measurements. As a consequence, the calibration of a secondary pressure gauge for static pressure experiments was made possible.

Dynamic experiments involve the fabrication of a specially shaped projectile that is propelled at high velocity to impact with a thin slab of sample. The slab of material contains slots at different known depths that hold flash blocks. These blocks glow when a perturbation, propagated as a shock wave, is encountered. A time-dependent photograph records the time between glows. Thus the

shock velocity, u_s, can be calculated and the density of the material estimated. Pins or other blocks can be used to measure the projectile velocity, u_p, before impact. These measurements can then be used to calibrate secondary pressure gauges or offer corroborating evidence for the static compression data.

To correctly analyze the shock compression data, the Rankine-Hugoniot equations were developed. "These equations relate the pressure, P, internal energy, E, specific volume, V, (or density ρ) behind the shock wave to the same quantities (denoted with the subscript 0) in front of the shock wave in terms of the shock velocity, u_s, and the particle velocity, u_p, due to the shock wave."[6]

The following series of equations are developed from the conservation laws, of mass, momentum, and energy respectively:

$$\rho_0 u_s = \rho(u_s - u_p) \qquad (1.12),$$

$$P - P_0 = \rho_0 u_s u_p \qquad (1.13),$$

$$\left(E - E_0 - \frac{u_s^2}{2}\right)\rho_0 u_s = P_0 u_p \qquad (1.14).$$

Now combining equations (1.12) and (1.13) and then solving for u_s and u_p leads to:

$$u_s = V_0\sqrt{\frac{P-P_0}{V_0-V}} \qquad (1.15),$$

$$u_p = \sqrt{(P-P_0)(V_0-V)} \qquad (1.16).$$

Now substitute equations (1.15) and (1.16) into (1.14). This leads to the Hugoniot energy equation:

$$E - E_0 = \frac{(P+P_0)(V_0-V)}{2} \qquad (1.17).$$

Thus the measurement of any pair of variables listed in equations (1.13)-(1.17) and knowing the initial conditions will allow a determination of a point on the Hugoniot. The most common pair of variables measured are the shock and particle velocities. In the absence of a phase transition, the relation between u_s and u_p is, for most materials, a linear one:

$$u_s = c_0 + s u_p \qquad (1.18).$$

It is usually not possible to directly measure the temperature of the material behind the shock wave. Therefore it is necessary to use the thermodynamic identity:

$$\frac{dT}{T}=-\gamma\frac{dV}{V}+\frac{dS}{C_V} \qquad (1.19).$$

Where T is the temperature C_V is the specific heat at constant volume and γ is the Grüneisen parameter:

$$\gamma=V\left(\frac{\partial P}{\partial E}\right)_V \qquad (1.20).$$

If the isentropes ($\Delta S=0$) have been found then the calculation for T is trivial. When this is not the case, the temperatures must be calculated directly along the Hugoniot. Equation (1.6) when coupled with

$$dE=TdS-PdV \qquad (1.21)$$

leads to an equation for the entropy along the Hugoniot:

$$2TdS=(V_0-V)dP+(P-P_0)dV \qquad (1.22).$$

Using the values along the Hugoniot with the known values of the specific heat and Grüneisen parameter, the coupled differential equations (1.19) and (1.22) may be integrated to give the temperature and entropy.

To be able to use these results to develop a primary pressure gauge for static high pressure research, it is necessary to know how the volume changes with pressure while the temperature remains constant. The easiest way of doing this is to calculate the thermal pressure P_T from the Hugoniot and subtract this value from the Hugoniot pressure, the total pressure:

$$P_T=\gamma\frac{E_T}{V} \qquad (1.23),$$

where E_T is the thermal energy. Using the Debye theory, the value for the thermal energy is calculated from:

$$E_T=3nk_BTD_3(x) \qquad (1.24),$$

$$D_3(x)=\frac{3}{x^3}\int_0^x\frac{z^3}{e^z-1}dz \qquad z=\frac{\theta}{T} \qquad (1.25),$$

where θ is the Debye temperature of the material.

Using shock compression data and the outlined formalism, isothermal equations of state were constructed for materials such as gold, molybdenum, tungsten and copper. These materials are commonly used as primary pressure gauges in static high pressure experiments because they are simple materials (i.e. having a cubic structure), and they do not undergo phase changes up to very high pressure.

Recall that early on in the derivation of the Hugoniot, an isothermal EOS can be developed from the Hugoniot. This EOS could then be used to calibrate a static secondary pressure gauge. For instance, it is well known that the R fluorescence peaks wavelengths of ruby will change with pressure. Thus it is a simple procedure to calibrate this change in wavelength with an EOS of a known material such as gold or other various elements. The ruby, for reasons that will be discussed in greater detail in section 2.3.1, is a commonly used pressure gauge in high pressure research.

§1.4 Structures of the Transition Metal Oxides and their Pressure Dependence

1.4.1 Monoxides

All the 30 monoxides known can be divided into 5 categories depending on their structures at room conditions:[7]

i)	Gaseous:	CO
ii)	Litharge (tetragonal):	PbO, SnO, PdO, PtO
iii)	Wurtzite (HCP):	BeO, ZnO
iv)	Tenorite (monoclinic):	CuO, AgO
v)	Rocksalt (FCC):	SrO, BaO, and all the other monoxides.

The packing fraction is a useful quantity to compare structures of different compounds. It is defined as the ratio between the molar volume and the cube of the mean nearest neighbour cation-anion distances.[8] The packing index for the monoxide compounds decreases as the categories in the list above are descended. Since CO is a gas, it can not be included in this generalization.

Of the monoxides crystal structures, the least compact is litharge and the most compact is rocksalt. Based on compaction, it is expected that a litharge structure will transform to a wurtzite structure, a wurtzite structure to a tenorite structure, etc. In the case of ZnO, a transformation from the wurtzite-type structure to the rocksalt-type structure is observed at 10 GPa.[7] Furthermore the rocksalt-type structure of ZnO transforms to the CsCl-type structure at approximately 65 GPa.[7] It is also known that the larger rocksalt structures, adopted by BaO and SrO, transform to a smaller volume tetragonal (PH_4I) structure, (resembling a distorted CsCl-type structure) with a c/a ratio of 0.727 and a positional parameter, u, of 0.40. The positional parameter indicates the location of the anion in the given structure. The undistorted CsCl structure has a c/a ratio of 0.7071 and a positional parameter, u, of 0.50.[7] This is shown in Figure 1.1, where a circle indicates the molar volume and cube of the cation-anion distance of the monoxide. A closed circle represents

measurements done under room conditions, whereas measurements done at some pressure are shown as a dashed line to an open circle. This relationship between compounds of like structures, is due to the fact that when the molar volume is plotted against the cube of the anion-cation interatomic distance for different compounds, the slope of the line connecting the compounds of like structures is equivalent to the structure's packing fraction.

Table 1.1: Packing fraction for chosen crystalline structures.[7]

Structurbericht	Structure Type	Packing Index	c/a
A2	BCC	0.4636	
A1	FCC	0.4259	
B1	rocksalt	1.2045	
C1	fluorite	1.8545	
	hexagonal	0.4478	1.550
A3	HCP	0.4259	1.633
	hexagonal	0.4225	1.850
B10	litharge (PbO)	2.0	
B4	wurtzite (ZnO)	1.8	
	tenorite (CuO)	1.7	

At room temperature CuO forms a monoclinic lattice with lattice parameters **a**=4.6835 Å, **b**=3.4226 Å, **c**=5.1288 Å, and β=99.54°. The space group is C2/c with a y-parameter, describing the position along the b axis, equal to 0.4139.[9] The positions of the 4 Cu atoms in the unit cell are given by (1/4,1/4,0), (3/4,1/4,1/2), (3/4,3/4,0), (1/4,3/4,1/2), while the 4 O atom positions are given by (0,y,1/4), (0,-y,3/4), (1/2,1/2+y,1/4), (1/2,1/2-y,3/4). There has been no phase transition reported up to 50 GPa, which is to date, with the exception of the present work, the maximum pressure reported by high pressure experimentalists.[10]

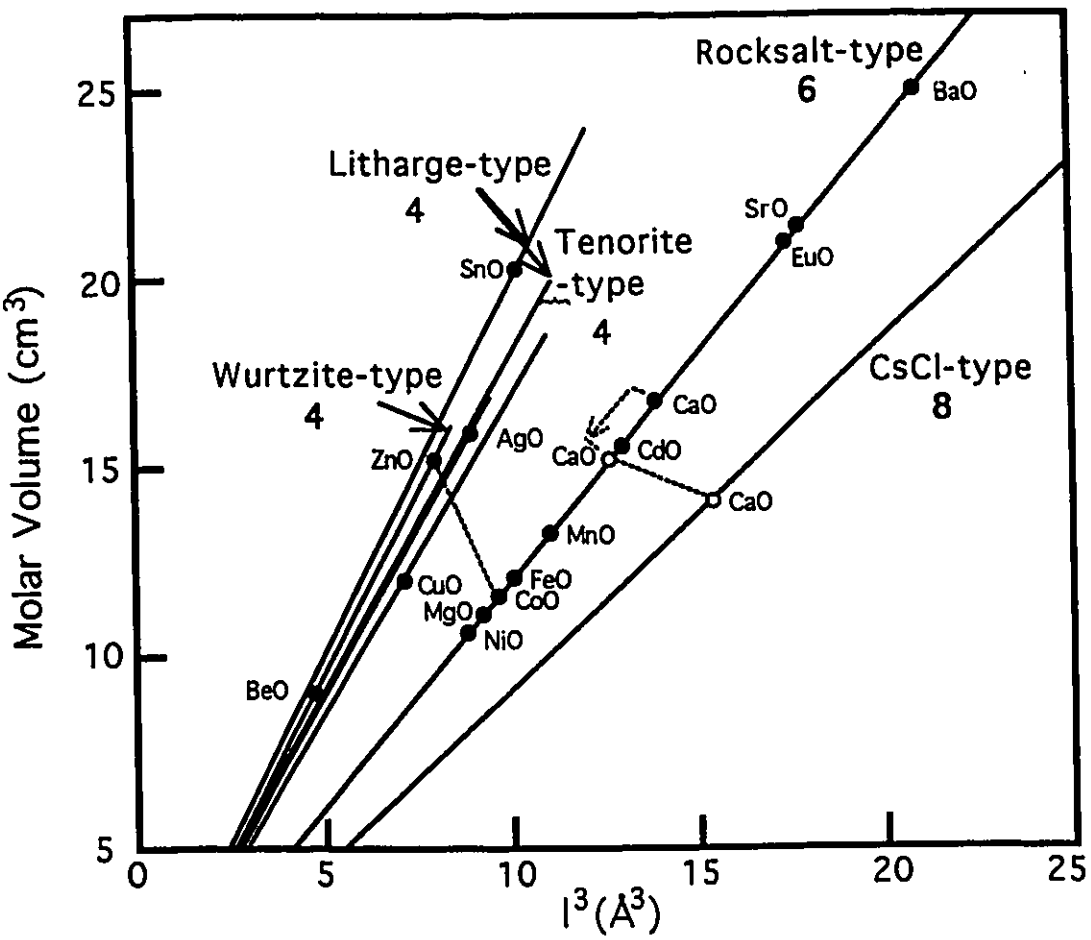

Figure 1.1: Molar volume versus the cube of cation-anion distance of monoxides.[7] The dashed lines represent transitions from the room condition measurements (closed circles) to those done at some pressure (open circles). The number indicates the coordination number of the structure that is directly above it.

As pressure is increased the lattice parameters for the monoclinic structure change: the **a**-parameter increases, while **b** and **c** decrease and the angle β increases. Although it would seem surprising that the **a**-parameter would increase, this occurrence has been seen in other monoclinic structures such as in the case of γ-PbO or SnO structure at pressures above 1 and 2 GPa respectively.[11] When the volume is calculated from the lattice parameters, it consistently decreases with pressure, as expected. A neutron diffraction study has shown that along with the changing parameters, the atomic placements inside the lattice also change. Unfortunately due to experimental constraints, this study could only be accomplished to a pressure of 2.2 GPa.[12]

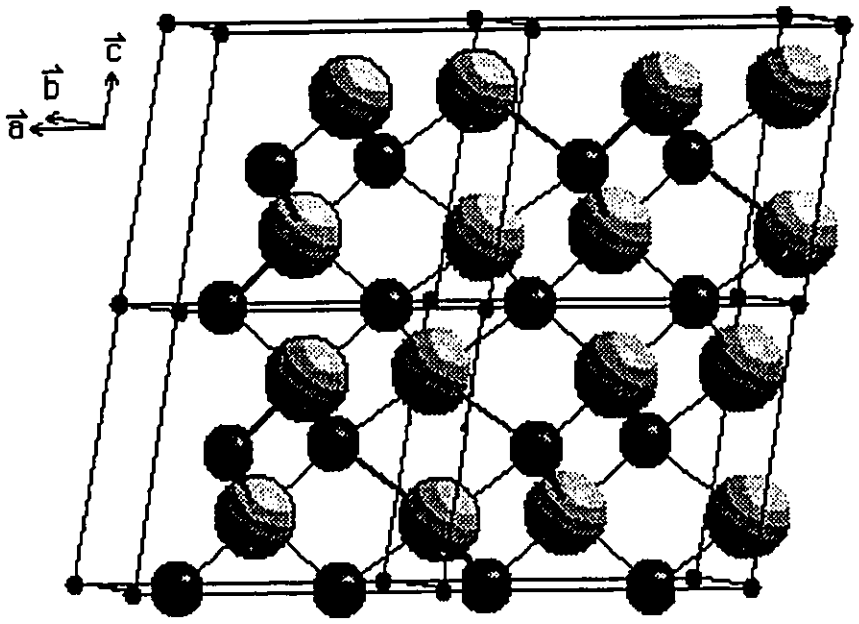

Figure 1.2: The monoclinic crystal structure of CuO at room pressure. The copper atoms are represented by the larger balls, and oxygen atoms by the smaller ones.

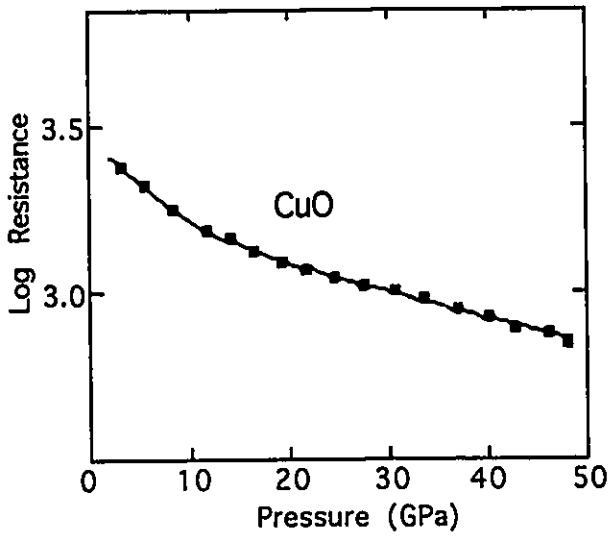

Figure 1.3: Log resistance versus pressure for a sample of CuO.[13]

There has been a report of a change at 10 GPa using resistivity measurements. However the researchers had concluded that no transitions were observable. At this pressure a change in the slope is visible in a logarithmic graph of resistance versus pressure[13] (see Figure 1.3). There is however another possible explanation other

than a phase change to explain this change in the slope. At approximately 10 GPa the lattice parameter **a** of the monoclinic structure ceases increasing and starts to decrease (although it has been noted that this could indicate a yet undiscovered phase change). This change in the behaviour of the a-parameter could be correlated with the change in the slope of the resistivity curve. One report alluded to a phase transition in a single crystal of CuO at 10 GPa. The authors believed that the new space group is monoclinic Cc, which is a transition from the monoclinic C2/c group at room pressure.[10] This report has yet to be published. It should also be noted that the noted changes are occurring at 10 GPa which, as will be shown later, is close to the freezing point of methanol-ethanol, which is often used as a pressure transmitting medium. The freezing of the pressure medium results in non-hydrostaticity inside the pressure chamber, which could affect the measurements.

Recall that one of the motivations behind copper-oxide research is due to the constant reoccurrence of these elements in the production of high-T_c superconductors. Thus an obvious research project, that was undertaken by Bourne et al.[14], was to make electrical conductivity measurements on copper oxides at different temperatures and pressures. During the course of their investigation, no discontinuities in the resistance measurements vs. pressure or temperature were observed. The sample of CuO was studied to 60 GPa and 3000 K with no phase changes visible.

Reimann and Syassen also reported[15] a "phase transition" at 10 GPa. The experiment was conducted with a gasketed diamond anvil cell using paraffin oil or CsCl as a pressure medium. Raman spectroscopy was used to probe the lattice structure while ruby fluorescence was used as a pressure calibrant. The peaks for the 3 phonon lines labeled, A, B, and C increased in wavenumber as the pressure was increased. Upon release of the pressure there appeared to be some scatter in the peak energies of A and B while there was a definite change in the energy value for C at 0 GPa as shown in Figure 1.4. Although this fact is important it does not necessarily

mean that a phase change has occurred as reported. Another research group[10] has shown that when pressure is applied to CuO there is a relaxation of the structure with time. If this was not taken into account in the Raman spectroscopy experiment, it could possibility explain the hysteresis.

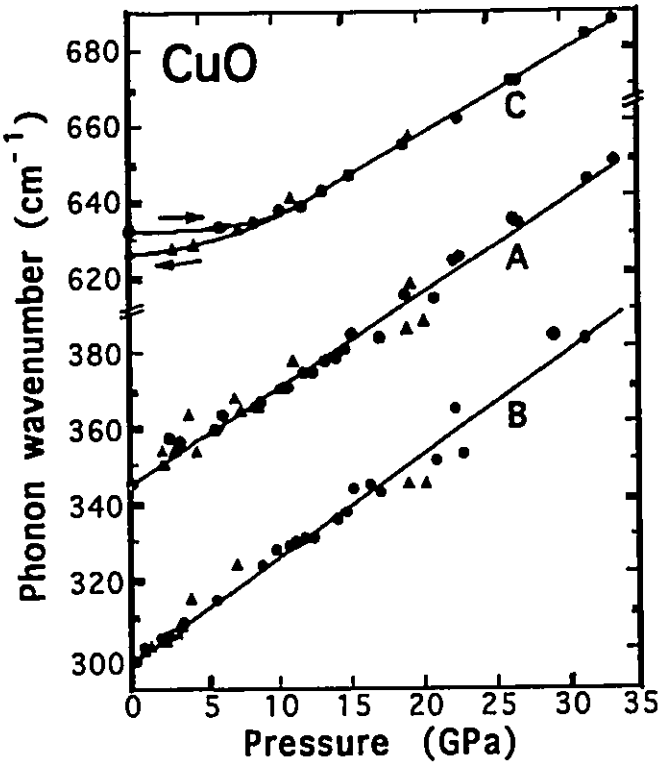

Figure 1.4: Pressure dependence of the Raman modes in CuO. Experimental values are denoted by circles for increasing pressure, by triangles for decreasing pressure. The solid lines are linear fits (for A and B and for C above 10 GPa) or a guide to the eye (for C below 10 GPa).[15]

1.4.2 A_2O Compounds

There has been very little research done on the A_2O compounds except in the case for H_2O and D_2O which have, since the start of high pressure research, been studied extensively. Of all the A_2O compounds, Cu_2O, Ag_2O and B_2O are the only compounds of this type that have been studied to high pressure.

Both Ag_2O and Cu_2O form a cubic structure (cuprite) at room conditions. Ag_2O undergoes a phase transition to a hexagonal phase at 0.4 GPa, this transition is similar to the one undergone by Cu_2O at

10 GPa. Ag_2O has been studied up to a pressure of 24 GPa and there is no indication of a third phase change. Cu_2O however, does undergo an additional phase transition at approximately 13 GPa to a different hexagonal structure. Due to the lack of data on A_2O compounds in general, no reliable prediction for a yet undiscovered phase transitions of Cu_2O can be made.

Cu_2O naturally occurs in a cubic structure with a lattice parameter of a= 4.2696 Å and space group Pn3m. Werner and Hochheimer[16] have shown that Cu_2O transforms to an hexagonal structure at 10 GPa with a lattice spacing of a= 2.90 Å and c= 19.31 Å. Another transition occurs at 18 GPa to a different hexagonal structure with lattice spacing of a= 2.82 Å and c= 12.70 Å with the $CdCl_2$ structure. This second hexagonal structure is observable to a pressure of 24 GPa, the highest pressure attained thus far by other researchers.[16]

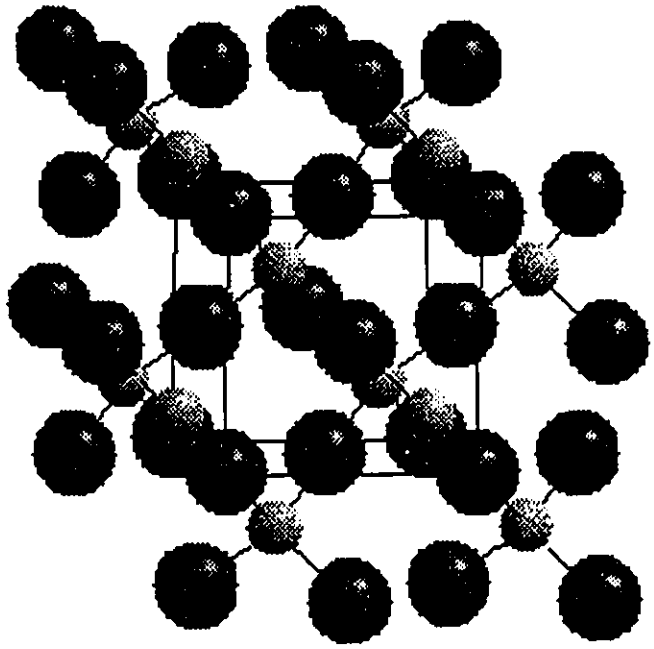

Figure 1.5: The cubic crystal structure of Cu_2O. The copper atoms (large balls) form a FCC lattice interlaced by a BCC lattice created by the oxygen atoms (small balls).

Having discussed the basic concepts of the research project we are now prepared to discuss the experimental aspects of the research project. The apparati used to investigate the pressure behaviour of CuO and Cu_2O will be introduced and their merits will be discussed. This will allow a thorough analysis of the data recorded from the devices used. The study of CuO and Cu_2O was undertaken to a maximum pressure of 60 GPa and 35 GPa, respectively. This research project surpassed both sample's maximum pressure reported by other research groups. It also surpasses the highest pressure of 40 GPa reported by us[17] in 1993. This will allow a verification of the results mentioned above on the two compounds. It will also allow for the possibility of discovering a new phase transition at a pressure that has yet to be attained.

§2 Experimental Apparatus

§2.1 Diamond Anvil Cell

The first high pressure anvil device, "the Bridgeman anvil cell" developed by P. W. Bridgeman, used tungsten-carbide anvils to apply pressure to the sample.[18] This device, invented nearly 80 years ago, was used until 1950 to investigate the compressibility and electrical resistivity of solid substances at varying pressures. This anvil cell design was capable of producing a maximum pressure of 10 GPa (1 GPa=10 kbar). Drickamer and co-workers then developed the Drickamer cell, which was capable of obtaining a few tens of gigapascals. The Drickamer cell was used for Mössbauer resonance, X-ray diffraction, and optical absorption studies.[2] Later Weir and Van Valkenburg improved on this device by replacing the tungsten-carbide anvils with diamond anvils.[19] The modern diamond anvil cell (DAC) has seen little change from the ones developed by Weir et al.

There have been minor changes to the DAC, such as beveled washers in place of the spring and a longer lever. These technical refinements have allowed researchers to obtain and surpass pressures of 40 GPa. The DAC has the following two components which are shown in Figure 2.1: two opposing diamond anvils pressing in towards each other and the metallic gasket which houses the pressure chamber. High pressure physicists studying a selection of elements, most notably hydrogen, have attained during their investigations, pressures in excess of 200 GPa.[20] To attain such a high pressure, experimentalists use opposing diamond anvils with beveled culets, tungsten-carbide supports and a high

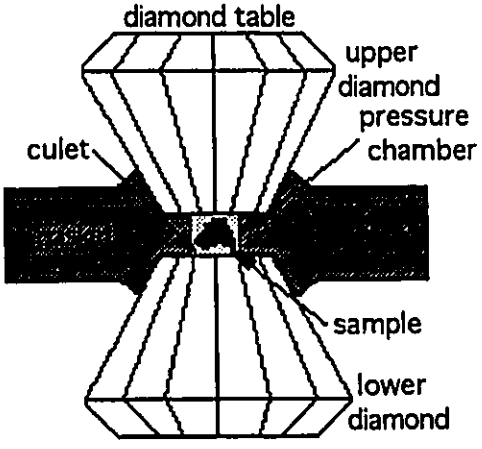

Figure 2.1: The nucleus of the DAC: two opposed diamonds with a gasket for sample confinement.

yield strength metallic gasket. Two common types of supports are shown in Figures 2.2 and 2.3, their use will be discussed shortly.

Today the most commonly used DAC in high pressure research, is the Mao-Bell DAC (see Figure 2.4). This cell has conical openings of approximately 8° in the top and bottom rockers. There are also 8° conical openings in the top of the outer cylinder and the bottom of the piston. In addition to the conical opening, a thin slit opening of approximately 20° is found at the top of the DAC and the upper seat as shown in Figure 2.2. The slit allows X-ray diffraction spectra to be taken at an angle greater than would be possible through the use of the conical apertures. Unlike a larger conical opening, the slit does not seriously jeopardize the structural integrity of the DAC. Two DACs, based on the Mao-Bell design, were used in this series of experiments on CuO and Cu_2O; they are referred to as the LP DAC (low pressure) and HP DAC (high pressure).

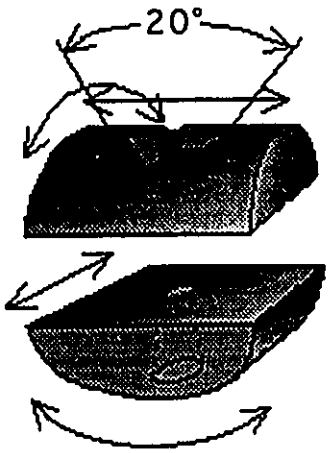

Figure 2.2: The lower and upper rockers for the LP DAC. Except for the arrows indicating the angle of the slit, all the other arrows indicate in which direction the rocker is allowed to move.

The LP DAC has two 1/4 carat type IA, 8 facet gem quality diamonds, with 500 μm culets. The diamonds sit on two half cylinder rockers that translate and rotate perpendicular to each other. This allows translational centering and leveling of the diamonds in relation to one another. Unleveled anvil flats will cause stress gradients to occur across its surface. This could lead to the occurrence of two complications: first, these stresses would create a non-hydrostatic environment, resulting in a change in the EOS of the sample and second, these stresses are maximum at the edge, which unfortunately is the weakest point of the diamond anvil face. Thus the likelihood of diamond anvil fracturing is increased and subsequently the maximum pressure that can be attained with the DAC is decreased. If the anvils are unleveled there is the additional possibility that the sharp edges on the circumference

of the diamond anvils may cut through the gasket material, thus coming into contact with one another. This would prevent further pressure increases and is another circumstance that could result in an anvil fracture.

Leveling of the diamonds was done by tapping on the edge of the rocker while verifying the result by the observation of Fizeau interference fringes of the quasimonochromatic light (from a sodium lamp) between the two diamonds. The leveling was considered satisfactory when only one fringe was visible across the tip. This procedure allowed the leveling of the diamonds to be accurate to within 0.4[mm]/1[m]. The LP DAC was used to study samples up to 30 GPa.

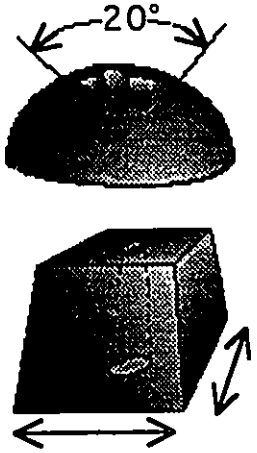

Figure 2.3: The lower and upper seats for the HP DAC. Except for the arrows indicating the angle of the slit, all the other arrows indicate in which direction the rocker is allowed to move.

The HP DAC has two 1/4 carat type IA, 16 facet gem quality diamonds, with 300 μm culets. The bottom diamond sits on a truncated pyramid shaped tungsten carbide seat. Four screws were used to translate the bottom diamond in the horizontal plane, allowing it to be centered with the top diamond. The pyramidal shape prevented the possibility of the seat slipping out of its holder. The top diamond sat on a tungsten carbide hemisphere with screws pushing on four slanting slots to allow the diamond to be leveled in relation to the bottom diamond culet. By moving the piston up and down, the width of the interference fringe could be estimated. The diamonds were routinely leveled to an accuracy greater than 1[mm]/1[m]. Quite often, near perfection in leveling was attained when the interference fringes were seen to begin at the center of the diamond and work their way out in a circle to the edges of the culet as the bottom diamond was moved towards the top diamond. This DAC was used to study the pressure dependence of samples up to 60 GPa.

Originally gaskets were not used in high pressure anvil devices and this omission allowed the sample to have some freedom of movement along the diamond culet. This resulted in a uniaxial stress to occur across the sample's surface. Housing and sealing the sample inside a gasket created a quasi-hydrostatic environment.[2] This was due to the gasket closing around the sample and pressing towards the center as the pressure inside the chamber was increased. The gasket would also act as a barrier to prevent the diamonds from coming into contact with one another.[2]

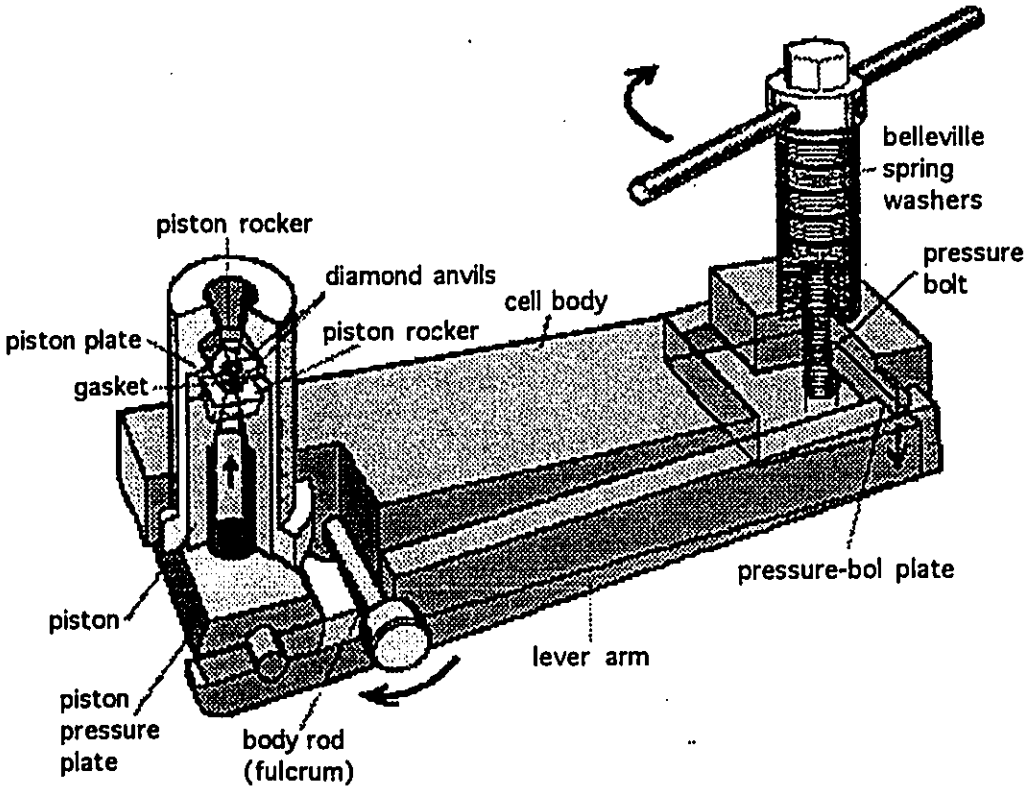

Figure 2.4: The DAC and lever arm used to create pressures on samples of interest.

The gasket material used in our study was AISI T301 hardened stainless steel gasket with the dimensions 8 mm x 30 mm and a thickness of 250 μm. The gasket was placed in-between previously leveled diamond anvils. Pressure was applied to indent the gasket to a final thickness of 80 μm. The gasket was removed and using a high

precision drill press, a hole was drilled in the center of the indentation.

Prior to replacing the gasket back onto the bottom diamond, the anvils were examined to ensure that they were still leveled, aligned and free of debris. The drilled gasket was correctly oriented on top the bottom diamond through the use of previously made markings on the gasket. Correct placement of the gasket ensured that it would sit flat on the face of the diamond and create a good seal with the anvil. A proper seal was necessary to prevent the sample from slipping under the gasket and the pressure medium seeping out through a gap.

§2.2 Pressure Transmitting Medium

To create a better hydrostatic environment at low to moderate pressure, a pressure transmitting medium may be used. A useful pressure medium would:

i) remain in a fluid form or be very compressible while it is in its solid phase to a high pressure,
ii) not chemically react with the sample,
iii) not diffract or absorb photons from the experimental probe (X-ray or laser light).

A common pressure medium is methanol:ethanol (M:E), mixed respectively at a 4:1 volume ratio. M:E freezes at a pressure of 10.4 GPa, but remains malleable to approximately 20 GPa.[2] (This will be shown in Section 3.1.) Hence M:E is a useful pressure medium for modest pressures. Silicone oil is another liquid that is used as a pressure medium, though not as frequently as M:E.

The noble elements form another class of pressure media, among which Ar and He are most frequently used. To load a usable amount, it is necessary to liquefy the gas first. Since nitrogen does not react easily with other elements and is a liquid only at a low temperature, it conviently mimics the behaviour of a noble gas. However, unlike the noble gases, nitrogen is inexpensive and readily available in its liquid form. At room temperature, nitrogen will freeze at 2.4 GPa but remains compressible to approximately 13 GPa.[2]

The loading of a cryogenic liquid by immersion requires the use of special apparati and techniques. A cover was fabricated to allow the top of the DAC to be flushed with dry argon while the DAC was cooled to the appropriate temperature. This prevented the diamond anvil table from becoming frosted and allowed a visual inspection of the chamber and the sample as the loading of the liquid was occurring. Once the liquid was viewed inside the chamber, the diamonds would be brought together to seal the chamber around the sample.[21] Since the DAC was not placed entirely in a dry atmosphere, condensation would rapidly cover the DAC's surface. Rust damage to

the DAC was minimized by immediately placing the sealed DAC into a desiccator. In spite of all the precautions taken to prevent rust, the damage was too great to warrant further attempts until the entire process of loading the cryogenic liquid could be done in a dry atmosphere.

Another option is not to use a pressure medium at all. This allows quicker and easier loading of the sample. However it has been shown that the lack of a pressure medium will cause the equation of state of a solid to be different from the measurements made with a pressure medium. The lack of a medium would cause the compressibility of the sample to be smaller than the value measured for a sample in a pressure medium.[22]

During this series of experiments various pressure media were used. Methanol-ethanol pressure medium was first used for two series of X-ray diffraction, in order to match the experimental conditions of two other research groups (Malinowski et al.[23] and in addition Åsbrink et al.[10]) who have used M:E exclusively in their research. Silicone oil was used and samples of CuO and Cu_2O were also studied without a pressure medium.

§2.3 Pressure Gauges

2.3.1 Optical

$Al_2O_3:Cr^{3+}$ is a preferred pressure gauge for a variety of reasons. It fluoresces strongly under laser illumination, thus little effort is required to achieve a satisfactory signal to noise ratio. It is possible to resolve a fitted fluorescence peak to with an error of 0.1 nm which is equivalent to a change in 0.25 GPa, resulting in a fairly precise pressure gauge.

The impurity Cr^{3+} in alumina replaces Al resulting in two new major absorption bands, $^4T_1$ at 400 nm (3.1 eV) and $^4T_2$ at 550 nm (2.25 eV) and another weaker band at 250 nm (4.95 eV) at room conditions in which photons can be absorbed. Thus the 514 nm Ar^+ laser line is quite efficient at exciting the fluorescence lines. The absorption band will red-shift as the pressure is increased. At approximately 157 GPa the fluorescence peaks are in the near infrared range (740 nm). The 29 wavenumbers difference between fluorescence peaks R_1 and R_2 is due to electron spin orbit coupling.

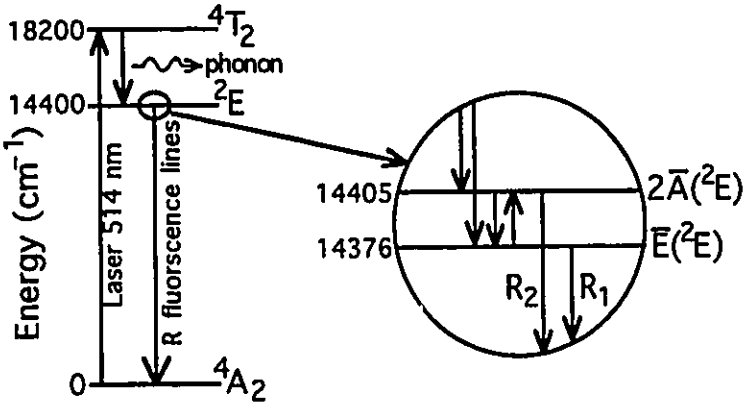

Figure 2.5 Absorption/emission energy diagrams of the R_2 and R_1 ruby fluorescence lines.

The relation between the wavelengths of the two major R fluorescence lines and pressure is well documented. The following equations were calibrated under hydrostatic conditions:

$$P(GPa) = \frac{\lambda(nm)-\lambda_0(nm)}{0.395} \qquad P \leq 30\ GPa \qquad (2.1),$$

$$P(GPa) = 248.4\left[\left(\frac{\lambda}{\lambda_0}\right)^{7.665} - 1\right] \qquad P \leq 150 GPa \qquad (2.2),$$

where λ is the wavelength of the ruby fluorescence of R_1 at some pressure, P, and λ_0=694.2 nm is the wavelength of the R_1 ruby fluorescence peak at room pressure.[24] Since all of the constituent elements of $Al_2O_3:Cr^{3+}$ have a small number of electrons, its X-ray absorption, diffraction and emission are low in relation to those elements that have a larger number of electrons. For these reasons it is an ideal pressure gauge for X-ray diffraction studies. Only a small mass of $Al_2O_3:Cr^{3+}$ is needed to achieve a satisfactory fluorescence signal for a pressure measurement. To measure the pressure it was necessary to excite the electrons of $Al_2O_3:Cr^{3+}$ using a laser and then analyze its fluorescence with a spectrometer.

2.3.2 Equation of State of a Material for use as a Pressure Gauge

The purpose of our work is to collect data on the pressure behaviour of a specific sample. The method used, was to accumulate data on the change of volume with pressure. Recall from Section 1.3.1 that an equation (third-order Birch-Murnaghan EOS) was derived. This equation relates the change of volume with pressure. The natural thing to do is to interpret the data by the chosen model.

Thus the data collected was compared to the third-order Birch-Murnaghan EOS model:

$$P=\frac{3}{2}B_0\left[\left(\frac{V}{V_0}\right)^{-\frac{7}{3}}-\left(\frac{V}{V_0}\right)^{-\frac{5}{3}}\right]\left[1+\frac{3}{4}(B_0'-4)\left\{\left(\frac{V}{V_0}\right)^{-\frac{2}{3}}-1\right\}\right] \qquad (2.3),$$

Recall that the Birch-Murnaghan EOS parameters are: B_0 (the atmospheric bulk modulus at room pressure) and B_0' (the change in the bulk modulus with pressure at room pressure). Both parameters are found by using a non-linear least squares routine or χ^2-minimization routine to fit the pressure versus isothermal volume experimental data to the EOS.

Our gasket material, AISI T301 stainless steel, was found to be quite useful as a pressure gauge. By taking a diffraction spectrum of the gasket surrounding the sample, it was possible to measure the approximate pressure inside the chamber.

The third-order Birch-Murnaghan EOS parameter values for the two pressure gauges used during the study are shown in Table 2.1.

Table 2.1: The Birch-Murnaghan equation of state parameters for the indicated pressure gauges.

Pressure Gauges	B_0 [GPa]	B_0'	Atomic Volume[a] [Å^3]
Mo (BCC)[25]	262.8	3.949	31.176
stainless steel[26] T301 (BCC)	220	2.93	11.9
stainless steel[26] T301 (HCP)	187	2.29	11.65

[a] Value is for the volume at room pressure and temperature.

Molybdenum, used as a pressure gauge for this experiment, was purchased from Johnson Matthey Company. Nominal purity is 99.9% by mass and the grain size is between 3-7 μm. The values for the EOS of Mo were calculated using the Hugoniot values found in Kinslow.[27] Recalling the equations from section 1.2.1, the shock compression data was converted to obtain volume versus pressure values at a temperature of 297 K. Fitting these experimental values to the third-order Birch-Murnaghan EOS, B_0 and B_0' parameters were obtained. These values were compared to dynamic experimental data obtained recently at the Los Alamos National Laboratory[25], see Table 2.2.

Table 2.2: Comparison of EOS parameters of Mo obtained from shock compression data attained from two sources.

Reference	B_0 (GPa)	B_0'
Los Alamos	262.8	3.949
Kinslow	266.8	3.867

The room pressure volume for Mo was measured from a X-ray diffraction spectrum taken using a X-ray diffractometer at the University of Ottawa and is in agreement with values obtained by others (see Table 2.3). The Mo powder was either mixed with the sample using a mortar and pestle or was placed on top of the sample, the sample being initially loaded in the compression chamber. In the case of Cu_2O, the mass ratio was 2.8:1 in favour of Cu_2O while CuO had a much larger mass ratio of 13.4:1 with respect to Mo. This would result in the major (110) Mo peak having an intensity half that of the major peak of the sample ((111) in both cases of copper oxides) in question at room conditions.

Table 2.3. Comparison of the lattice constant of Mo (BCC) from different sources.

Source	a (Å)
Pearsons[28]	3.1468
Mo sample	3.1475

A sample of the Mo purchased for the experiment was sent to the X-ray diffractometer facility at the University of Ottawa. An X-ray diffraction spectrum was taken and the cubic lattice parameter shown in the second row of Table 2.3 was calculated.

§2.4 X-ray Diffraction Using Synchrotron Radiation

The most effective probe for determining the structure of a solid is X-ray diffraction.
Bragg's Law states:

$$d_{hkl} = \frac{n\ \lambda}{2\ \sin(\theta)} \qquad (2.4).$$

This relation is used for angle-dispersive X-ray diffraction, where λ (wavelength of the X-ray) is held constant while measuring the intensity versus θ (the 1/2 detector angle from the incident beam). Bragg Law's can also be defined as:

$$d_{hkl} = \frac{hc}{2E\ \sin(\theta)} \qquad (2.5).$$

Energy Dispersive X-ray Diffraction (EDXD) is accomplished by recording the energy spectrum of the diffracted white X-ray beam from a powder at a constant value of θ. From equation 2.5, the value of E•d at some specific (hkl) is a constant. Consequently we only need to record the energy spectrum at some constant angle θ. EDXD studies were done at the Cornell High Energy Synchrotron Source (CHESS) where line B1 is dedicated to high pressure science. This beam line receives its X-rays from the acceleration of electrons inside the Cornell Electron Storage Ring. On occasion line D1 was used, this line has the same setup as line B1 but it receives its X-rays from the acceleration of positrons.

The equation for the photon intensity for a synchrotron is a function of the energy of the electron[29]:

$$I(E) = 1.256\text{x}10^{7}\ \gamma\ E\ G_1(y)\ \frac{\text{photons eV}}{\text{s mrad mA}} \qquad (2.6),$$

where γ is the energy of the circulating electron.

$$\gamma = 1957E(\text{GeV}) \qquad (2.7),$$

$$G_1(y) = y\int_{y}^{\infty} K_{5/3}(t)dt \qquad (2.8),$$

$K_{5/3}$ is a modified Bessel function of the second kind, and

$$y = \frac{h\nu}{h\nu_c} = \frac{E}{E_c} \qquad (2.9).$$

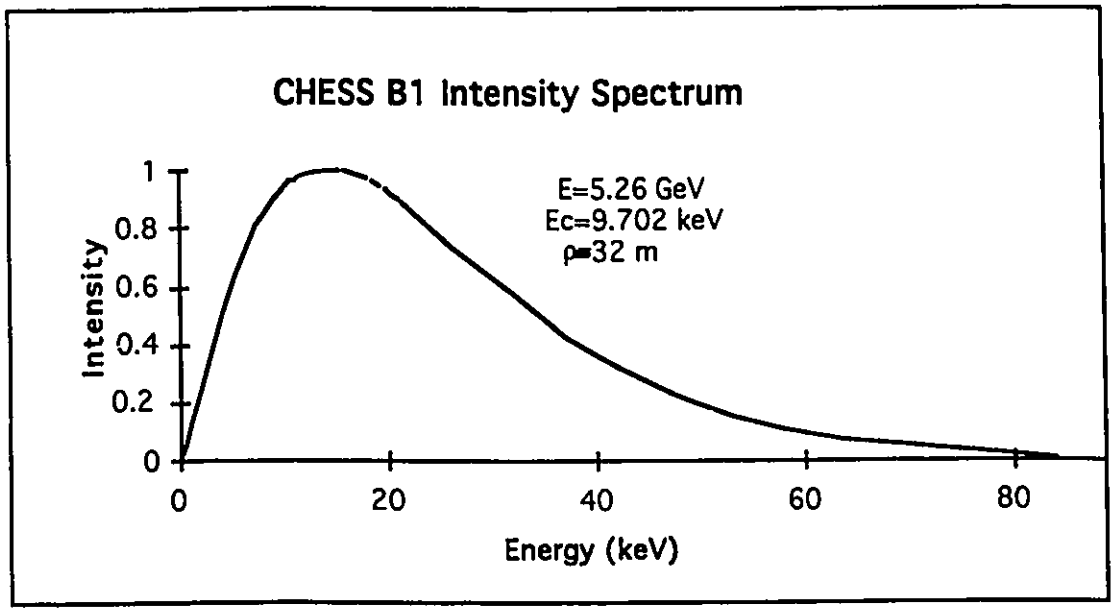

Figure 2.6: CHESS B1 line X-ray photon intensity spectrum from a bending magnet.

CHESS emits photons from 4 to 100 keV with a critical energy, E_c, at 10 keV, calculated from the energy of the circulating electrons, E=5.26 GeV,

$$E_c = \frac{3hc\gamma^3}{4\pi\rho} \qquad (2.10),$$

$$E_c(\text{keV}) = 2.218\frac{E^3(\text{GeV})}{\rho(\text{m})} \qquad (2.11),$$

where E_C is the critical energy and is defined as the energy at which half the irradiated power, P, is emitted at photon energies greater then the critical energy. ρ is the radius of curvature of the electron trajectory due to the bending magnets and can be calculated from:

$$\rho = 3.336\frac{E(\text{GeV})}{B(\text{T})} \qquad (2.13).$$

or as is more often the case ρ is fixed and the magnetic field of the magnet is changed to accommodate the desired energy value. In the case of CHESS the magnets have a bending radius of approximately 32 m. Figure 2.6 displays the intensity of photons in relation to their energy for the B1 line at CHESS.

Equation (2.6) is correct if there was no medium present between the electrons emitting X-rays and the sample under study. Unfortunately this is not possible, thus minor corrections must be made to take into account absorption of X-rays by various materials:
i) the Be window the X-rays passes through in order to exit the synchrotron ring,
ii) air as it travels towards the DAC,
and
iii) the diamond anvils.
that the X-rays travel through to illuminate the sample.

Although these corrections are minor, they are not insignificant and with some careful measurements and equipment design, reliable correction values can be found. Data refinement that is dependent on peak height (such as a Rietveld refinement) is difficult and the validity of the results uncertain. The main obstacle to such analysis is the inability of knowing whether there is preferred crystal orientation of the powdered sample. The design of the DAC, prevents an all angle diffraction from being done to remedy the crystal orientation problem. Although such analysis would be highly useful, the results that are obtained from the X-ray diffraction do allow a determination of the current lattice structure and its parameters at different pressures, which is very useful and is not possible with other probes such as resistance measurements or Raman spectroscopy.

To carry out the X-ray diffraction experiment a specially designed table allows the experimenter to move the DAC in the three Cartesian coordinates at micrometer intervals. Alignment of the sample with the collimated X-ray beam that has a cross-section of 2000 μm^2 is critical since the sample usually has a cross-section no greater than 4500 μm^2 and a thickness of 40 μm.

In addition there is a laser/spectrometric system designed for measuring *in situ* the R_1 and R_2 fluorescence peaks from $Al_2O_3:Cr^{3+}$.

The EDXD spectra were taken using an energy-sensitive Ge solid state detector that was set to a specific angle relative to the incident beam.

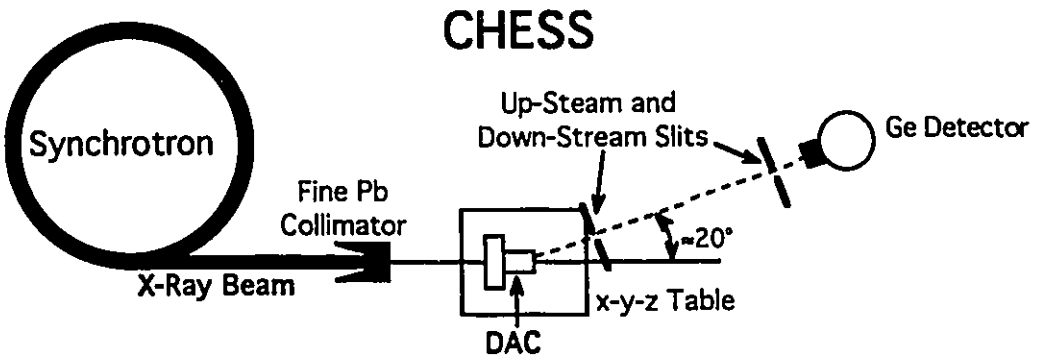

Figure 2.7: Experimental setup for Energy Dispersive X-ray Diffraction at CHESS.

Synchrotron radiation is used because of its high photon flux and inherent fine beam collimation. The strongest peaks in the diffraction spectrum usually appear in the 12-25 keV range, which is due to a number of factors. First, the intensity of the photons from the synchrotron is quite high in this region. Second, due to design considerations, the DAC slit has a maximum 2θ angle of 20° (see Figure 2.4), thus the high multiplicity lines such as 111 and 200 of a cubic structure with a lattice parameter in the 3-4 Å range, falls within the 12-25 keV range.

An X-ray collimator with a diameter approximately two-thirds the diameter of the pressure chamber would be selected. By choosing this diameter, it was possible to cover most of the sample without acquiring any signal from the gasket surrounding the sample. To locate the sample, the incoherently scattered photon beam passing through the DAC in the forward direction was measured using a PIN diode. When the X-ray beam was passing through the gasket material between the diamonds, a small flux was measured and as the chamber approached the X-ray beam, as a result of systematic sample search scans, the intensity of the transmitted beam would increase since the amount of material absorbing the beam decreased.

Once the sample chamber was centered on the beam, the table coordinates were noted and the PIN diode removed. A real time EDXD spectrum was then recorded using an energy discriminating detector. The detector was placed into the diffracted beam at an angle θ to the initial beam. The gasket peaks were identified and minimized by fine movements of the sample. Alignment along the X-ray beam was accomplished by measuring the rate with which the diffraction counts were taken. The optimal position occurred at the highest count rate. The DAC could then be removed and placed back into the beam to within 20 μm of the original position.

The angle at which the detector will record the spectrum was selected though the use of upstream and downstream slits as shown in Figure 2.7. The slits at CHESS were separated by a distance of 0.75 m and their individual widths ranged from 100-300 μm. The experimental error on the angle was then determined by using the equation:

$$\frac{\Delta(Ed)}{Ed} \approx \frac{a(1+b/a)}{2L} \cot\theta \qquad (2.14),$$

for a, b « L, where a and b are the widths of upstream and downstream slits respectively, L is the distance between the slits and θ is the angle at which the detector is placed relative to the initial beam. The detector is often placed at an angle of 12° and the slits were opened to a width of 200 μm yielding an absolute error of 0.150 keV Å on an Ed value of 59.304 keV Å.

The detector itself also has an intrinsic resolution that is dependent on the square root value of the energy it is attempting to discriminate.[30] This error is unique to each detector since it is dependent on the width, depth, and length of the crystal. The error was approximated by measuring the width of the fluorescence peaks across the energy range of 0 to 100 keV. At 6 keV the full width half maximum (FWHM) was 0.196 keV and at 80 keV the FWHM had increased to 0.420 keV.

Additionally the Ge detector will emit a much weaker peak that is exactly 9.8864 keV and for an extremely strong detected peak; another peak will also appear at 10.9821 keV lower in energy then the original peak. These peaks are commonly referred to as escape peaks. These values are the same values for the germanium fluorescence peaks $K_{\alpha 1}$ and $K_{\beta 1}$ respectively. Escape peaks are due to an absorption of photon energy by a bound electron equivalent to the fluorescence peak energy. Fortunately these escape peaks only appear for quite large peaks such as (111) or (11-1) of CuO in which escape peaks from 9.88 keV[31] fluorescence line was visible as shown in Figure 2.8. Only for the Mo $K_{\alpha 1}$ fluorescence peak was the second escape peak visible.

To calculate the angle at which the detector was placed in relation to the X-ray beam, an EDXD spectrum was recorded for a piece of gold foil placed where the sample inside the DAC was. To place the gold foil at the exact location as the sample, the diffraction signal was maximized, as was previously done with the sample. Knowing that gold has a face centered cubic (FCC) structure with a lattice constant of a=4.0786 Å[31], the d-spacings of the diffraction lines (111), (200), (220), (311), were calculated. Using these values and Bragg's law, the detector angle could then be calculated.

§ 2.5 Samples

A powdered sample of CuO with a purity of 99.999% by mass was purchased from Johnson Matthey Materials Technology. Impurities in the sample were tested for by observing the X-ray fluorescence peaks found by the energy discriminating detector. A diffraction pattern was taken using angular dispersive X-ray diffraction, which has a better resolution then EDXD, to test for the possibility of Cu_2O contaminating the CuO sample and vise versa. The room condition X-ray diffraction showed no peaks that could be attributed to Cu. The Cu_2O powdered sample had a purity of TMI 100 and was purchased from Spex Industries Inc.

For EDXD spectra, it was necessary to use a finely powdered sample. Enough fine powder was placed in the compression chamber of a DAC to occupy approximately 1/2 to 3/4 of the total chamber volume. Three different pressure gauges were used during the series of experiments on the copper oxide compounds. The element Mo was the gauge most often used. Although if ruby was be utilized as a pressure gauge, then one to three small $Al_2O_3:Cr^{3+}$ chips were placed in various locations inside the pressure chamber for use as a pressure gauge. A less effective method was to use the gasket edge as a pressure gauge. Once these procedures were completed a pressure medium, if one was desired, was introduced and the cell sealed.

The DAC was placed under a microscope for visual inspection of the pressure chamber. The pressure was increased and if the pressure chamber did not appear to be collapsing, then the pressure medium was still present inside the chamber. If $Al_2O_3:Cr^{3+}$ chips were being used, then an additional test was to illuminate the sample with a laser beam and observe the luminescence from the $Al_2O_3:Cr^{3+}$. This was possible by viewing the reflected beam through a Schott RG 610 colour filter that cuts off the 514.5 nm laser light but allows the $Al_2O_3:Cr^{3+}$ luminescence at 694.2 nm to pass through.

All X-ray fluorescence lines have been accounted for and there are no unknown peaks. Thus it is safe to conclude that the impurities that were present were negligible or consisted of Cu, O or the compound Cu_XO.

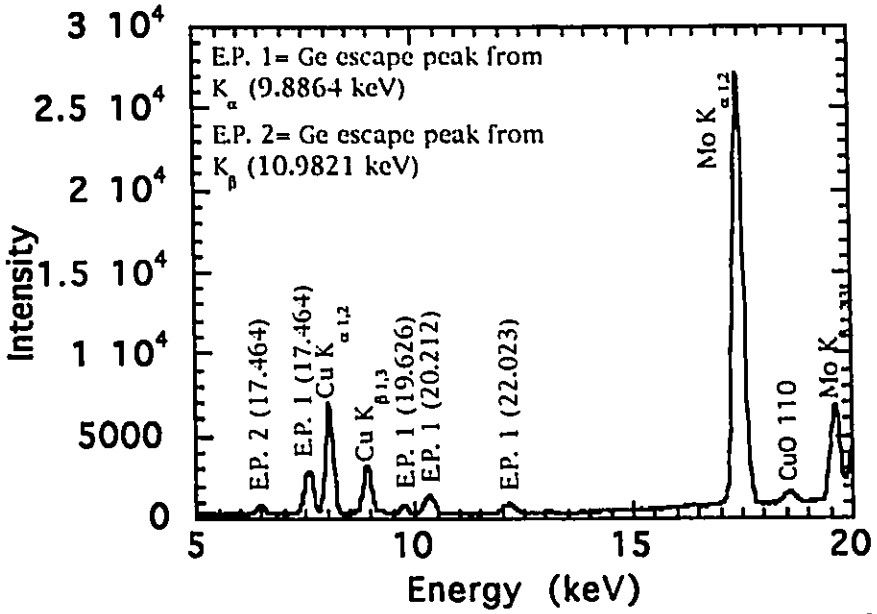

Figure 2.8: X-ray diffraction pattern of CuO sample at 0 GPa showing fluorescence lines.[31]

Over a span of a year and a half, three runs on cupric oxide were accomplished. In all three runs Mo was used as the pressure gauge. A hole approximately 250 μm or 150 μm across for the LP DAC or HP DAC, respectively, in the center of a previously indented stainless steel T301 gasket was used to contain the sample in a quasi-hydrostatic pressure environment. The lp3 and hp5 runs were accomplished without a pressure medium. The lp4 run in contrast was accomplished using a pressure medium of silicone oil. Due to design limitations the LP DAC in which lp4 and lp3 were accomplished was only used to a maximum pressure of 25 GPa. The HP DAC however was used to study the CuO sample to a maximum pressure of 60 GPa.

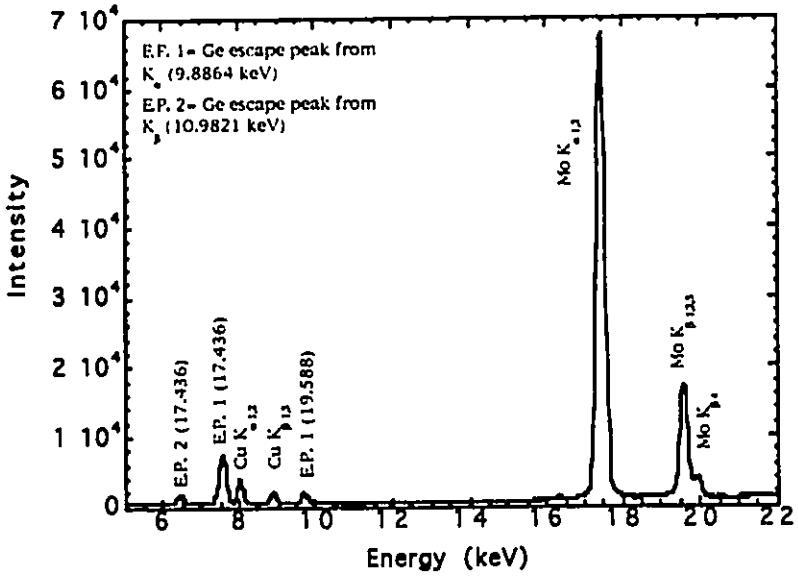

Figure 2.9: X-ray diffraction pattern of Cu_2O sample at 0 GPa showing fluorescence lines.[31]

§2.6 Data Analysis

A large number of spectra were recorded at CHESS for different samples at various pressures. To analyze this large amount of data in a systematic manner the program XRDA[32] was used. XRDA was invaluable in resolving peaks in a consistent manner, especially when 3 or 4 peaks were overlapping. Diffraction peaks were generally fitted with a Gaussian peak profile. After repeated observations, it was concluded that the Gaussian profile resulted in a better fit for most cases, rather than the Lorentzian profile normally used.

Once all necessary peaks were fitted, the characteristic peaks were identified and the Miller indices given. A fit of indexed peaks for the structure given was done by the program and the structure parameters calculated. If the atomic positions were specified, then a histogram of the diffraction intensities could be overlaid on top of the spectrum. In calculating the histogram, the program would take into account the synchrotron spectrum along with the absorption of the Be windows, air, diamonds and the sample itself.[32]

§3 Experimental Results and Discussion.

§3.1 Experimental Constraints and Error Considerations

§3.1.1 Chemical Transition in CuO

Earlier research done on the pressure dependence of CuO, used M:E (4:1 volume ratio) as a pressure medium.[23,10] To match the experimental conditions undertaken by these two groups, it was decided to use the same pressure medium. One other research group[15] had mentioned that due to a fear of a chemical reaction with CuO, their sample was loaded with a pressure medium of CsCl instead of M:E.

During the second run of the experiment at CHESS a chemical transformation from CuO to Cu was noticed. The M:E is suspected to have aided this chemical transformation. Figure 3.1 shows the expected peaks from a CuO sample at approximately 1.0 GPa. The same figure also shows an X-ray diffraction pattern of the same sample at 3.1 GPa. The new peaks fit quite well to an FCC structure with a lattice parameter of 3.596 Å. Elemental copper has a FCC structure with a lattice parameter of 3.6147 Å[28]. It is very unlikely that pure Cu was present with the CuO sample. Curiously, as the pressure was increased, the Cu's lattice parameter changed little. It was also noticed that the Cu appeared to be present before the first X-ray diffraction study was accomplished. In no other diffraction studies has pure copper appeared in the spectrum. Thus far no explanation has satisfactorily explained why there was no change in the lattice parameter of Cu as the pressure was increased and what mechanism allowed the transformation to occur.

In an attempt to prevent a reoccurrence of the chemical transformation, another pressure medium, silicone oil (704 diffusion pump fluid) purchased from Dow Corning Corporation was used. With silicone oil present, the X-ray diffraction signal to background ratio at low pressure was satisfactory. Unfortunately the signal degraded as pressure was increased. The degradation of

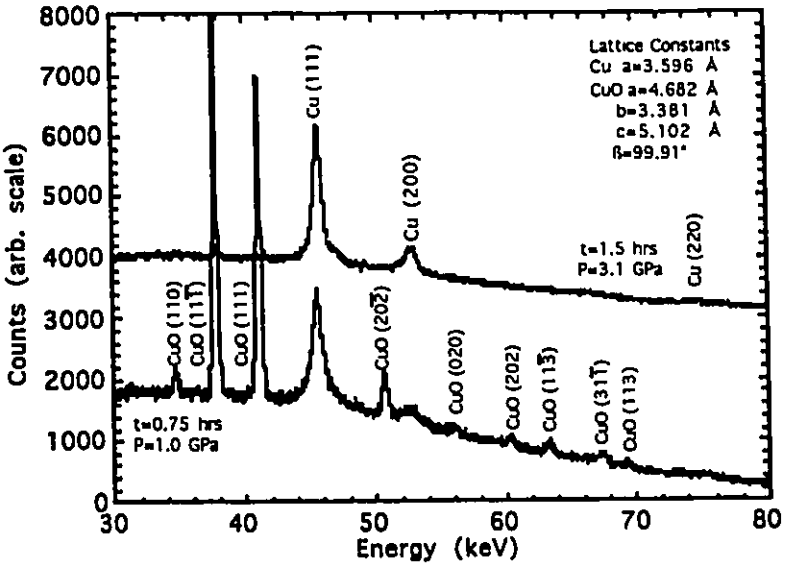

Figure 3.1: Two X-ray diffraction patterns of CuO in M:E. Both spectrums were taken of the same sample at the indicated pressures. The amount of time taken to record each spectrum is also noted.

the signal was also noticed when silicone oil was used as a pressure medium in the investigation of other oxides and not evident when those oxides were studied without a medium. Thus the degradation was attributed to the presence of the silicone oil in the pressure chamber. At 40 GPa, the background was too large to allow separation of the diffraction peaks from the background. This prevented accurate data on the lattice structure to be attained. As previously mentioned, there was an unsuccessful attempt to use a liquefied noble gas as a pressure medium. Finally, it was decided to study CuO and Cu_2O with no pressure medium.

§ 3.1.2 The Effects of the Presence and Absence of a Pressure Medium on a Sample.

Effects of a pressure medium or lack there of, on the behaviour of a sample under pressure is visible in the set of ruby fluorescence spectra in Figures 3.2 and 3.3. Notice that before the pressure is increased past 12 GPa, the two R-fluorescence peaks remain easily separable and their relative intensities remain unchanged. At 10.6 GPa[22] the M:E pressure medium becomes a

solid. The spectra shown in Figure 3.2b were taken at pressures above 12 GPa.

Figure 3.4a indicates that the R-lines separate gradually with pressure. Figure 3.4b shows the broadening of the fluorescence peaks with pressure. Unfortunately the broadening quickly overcomes any benefit of the separation of the two fluorescence peaks. Initially the absolute peak separation is 1.45 nm and increases by 0.35 nm to 1.80 nm, meanwhile the absolute broadening of the peaks collectively increases by 2.00 nm to a value of 3.00 nm from an initial value of 1.00 nm. Consequently the deconvolution of the two peaks becomes more uncertain, resulting in a less accurate measurement of the pressure.

The set of ruby spectra shown in Figure 3.3 were recorded without any pressure medium being present. The peaks quickly grew into one another, making deconvolution difficult. Note that the R_1-fluorescence peak became greater than the R_2 peak. This all occurred before the pressure of 6.6 GPa was reached. Recall that when a pressure medium was included, the peaks would not become inseparable until 20 GPa was surpassed.

To reiterate, the lack of a pressure medium results in non-hydrostatic forces to act on the sample. This may result in a change in the values of the measurements taken at a particular pressure, in comparison to a measurement taken with a pressure medium present. This was clearly seen in the spectra shown by comparing Figure 3.2a, 3.2b and 3.3. In addition non-hydrostaticity becomes worse after a pressure medium freezes. A sample of CuO with M:E being used as a pressure medium may result in slight changes in the measurements recorded before and after the solidification of the medium due to the non-hydrostaticity. This change in the measurements could lead one to conclude a phase change has occurred since a discontinuity in a measurement is one of the characteristics that indicates a phase transition.

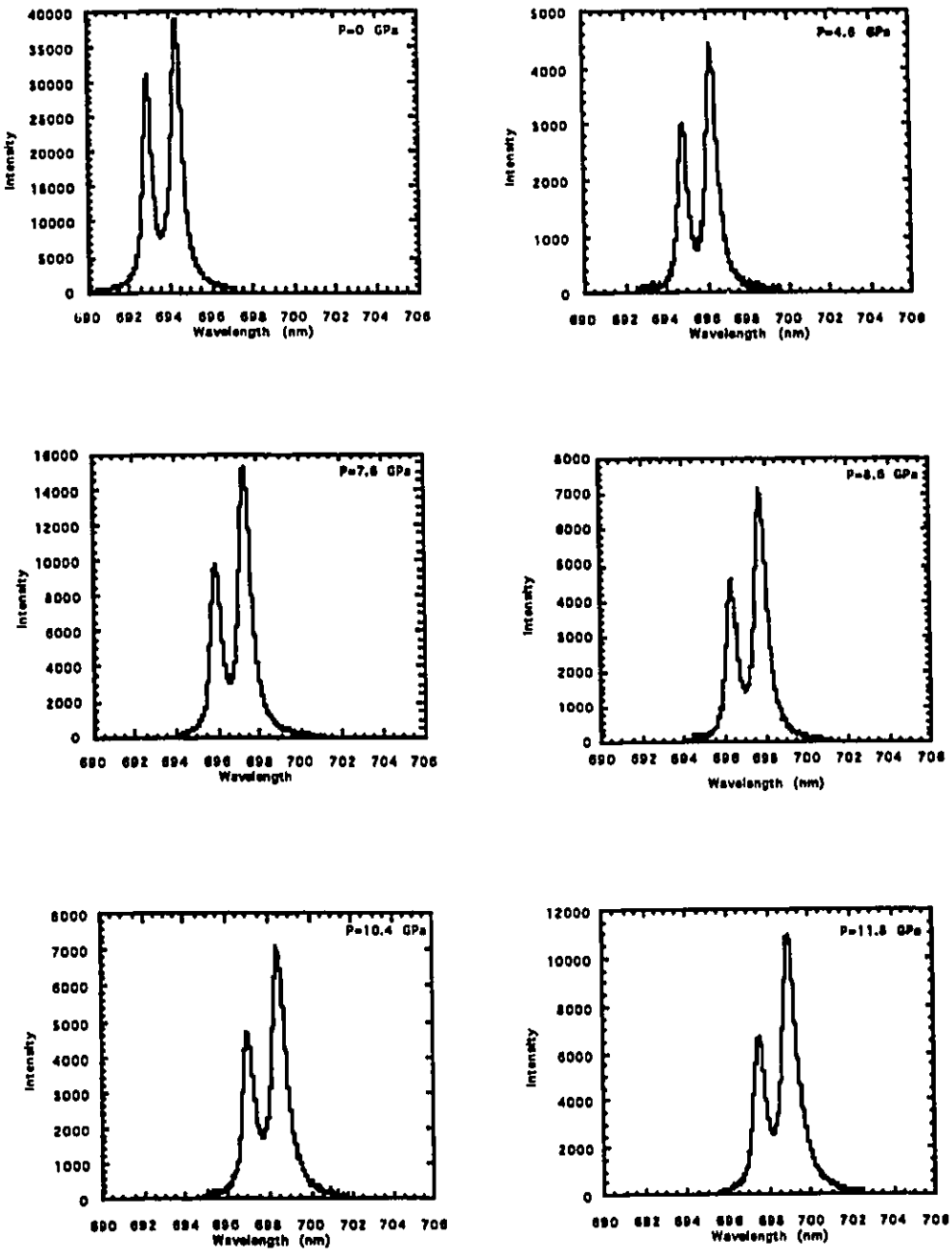

Figure 3.2a: The R_1 and R_2 fluorescence peaks taken of ruby at pressures below the freezing point of the pressure medium, methanol:ethanol, which was present inside the experimental chamber.

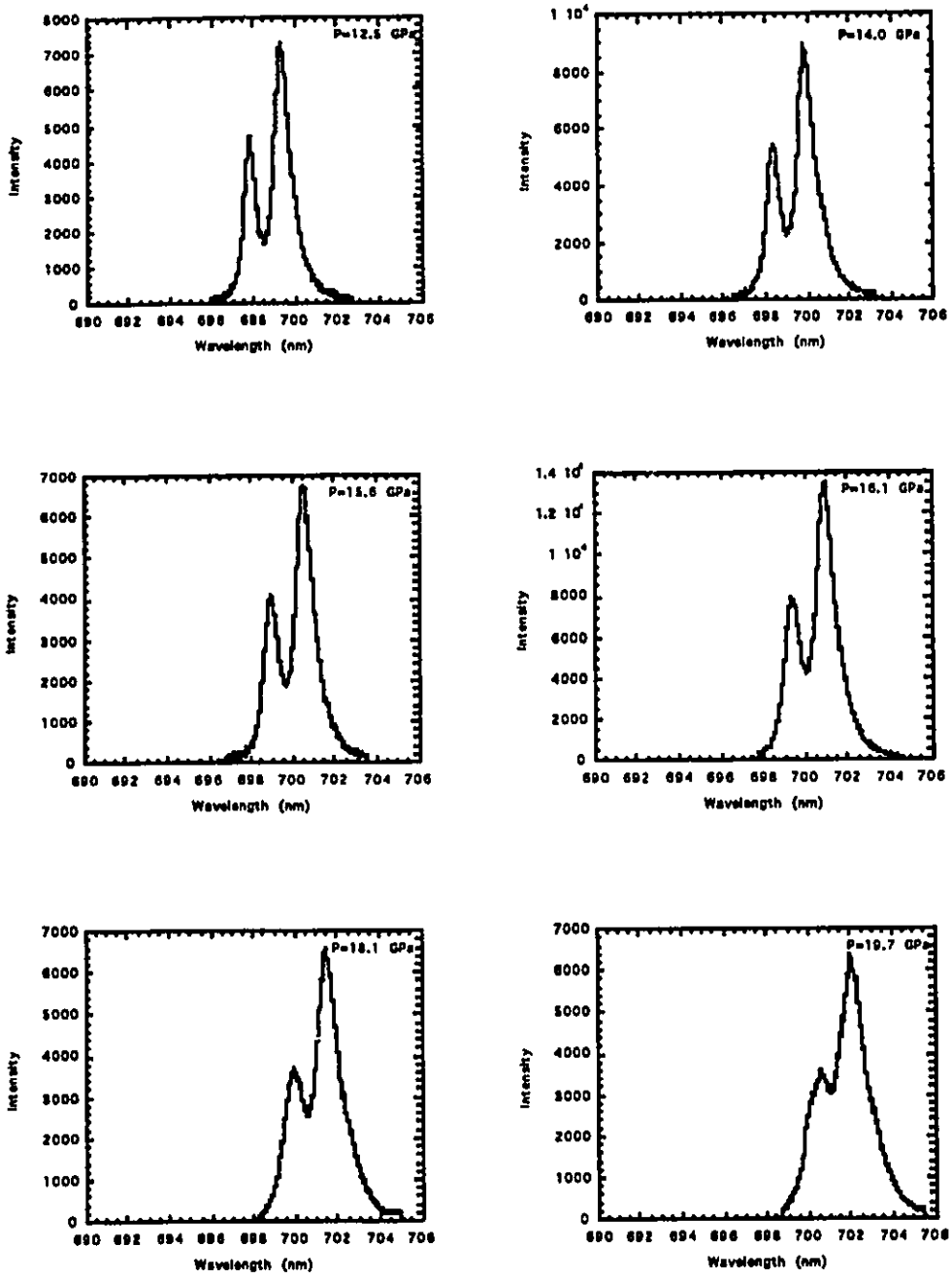

Figure 3.2b: The R_1 and R_2 fluorescence peaks taken of ruby at pressures above the freezing point of the pressure medium, methanol:ethanol, which is present inside the experimental chamber.

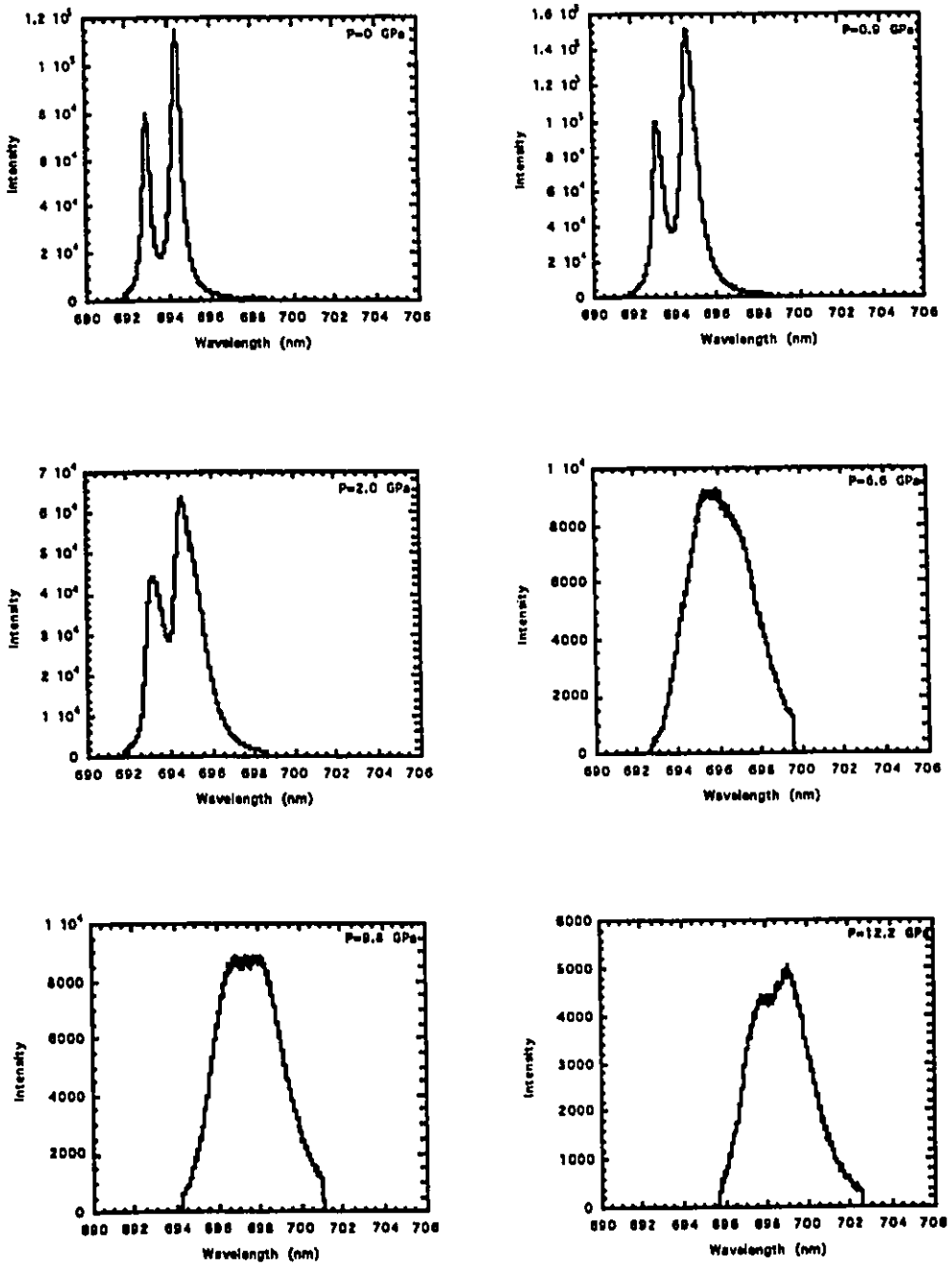

Figure 3.3: The R_1 and R_2 fluorescence peaks taken of ruby at various pressures with no pressure medium present inside the experimental chamber.

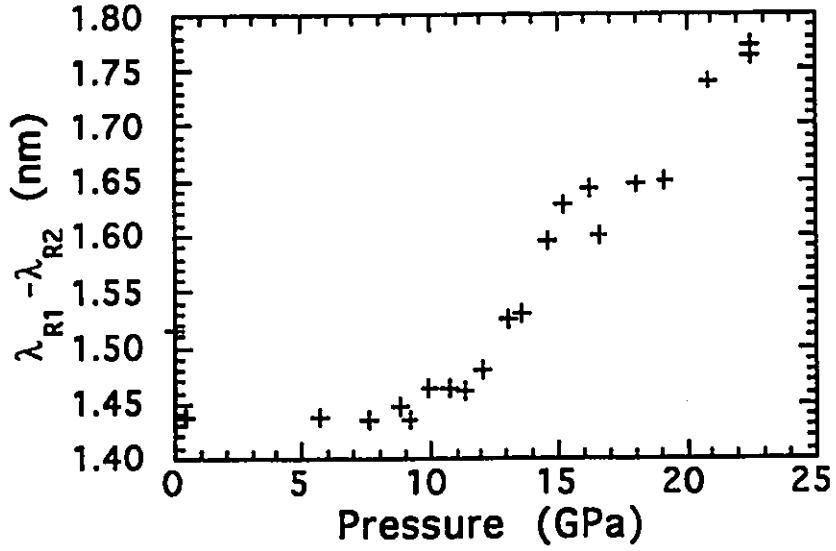

Figure 3.4a: Plot of the difference of the R_2 and R_1 fluorescence peak wavelengths versus pressure for a $Al_2O_3:Cr^{3+}$ (ruby) chip under quasi-hydrostatic pressure due to the use of a pressure medium of M:E (4:1).

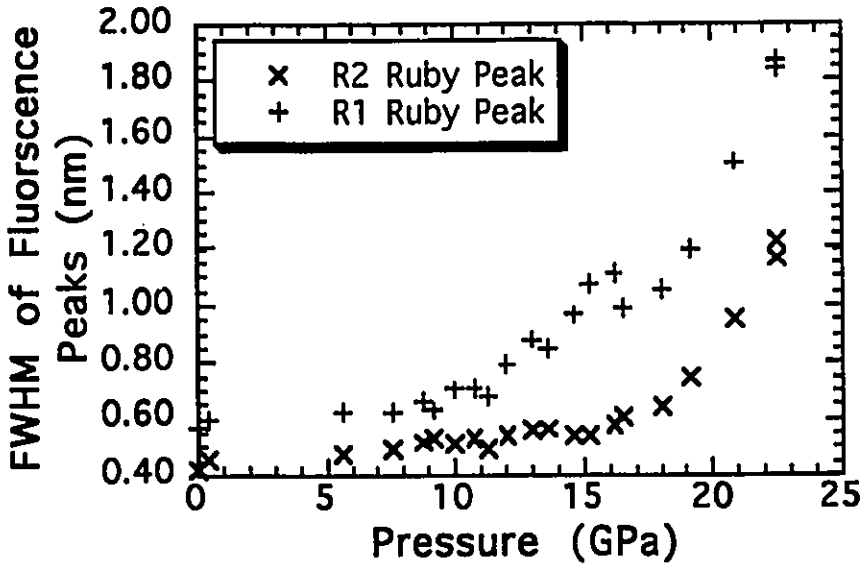

Figure 3.4b: Plot of the FWHM of the R_1, R_2 fluorescence peak energies versus pressure for a $Al_2O_3:Cr^{3+}$ (ruby) chip under quasi-hydrostatic pressure due to the use of a pressure media of M:E (4:1).

Two different research groups (Reimann and Syassen[15] and Åsbrink et al.[10]) have mentioned in their papers that they have seen evidence of a phase change at approximately 10 GPa. This is

the same pressure that the pressure medium methanol:ethanol, that they both used, freezes. Unfortunately both groups did not substantiate their conclusions with results, and no papers by either group about this phase transition has been forthcoming. As has just been mentioned, M:E freezes at approximately the same pressure that the phase transition occurs; one is left to wonder whether the reported phase change is due to the sample itself or just a result of the samples sensitivity to the non-hydrostaticity now present due to the freezing of the pressure medium.

§ 3.1.3 Search for a Suitable Pressure Gauges

The elemental pressure calibrants Au and Pt were examined in order to determine whether they would be suitable pressure gauge candidates. Due to the large number of peaks produced by a monoclinic structure, neither of these elemental pressure gauges had less of an overlap with sample peaks than Mo. Tungsten was also examined as a possible pressure calibrant but was rejected since it had the same BCC structure and a lattice parameter close to that of Mo resulting in nearly identical peak overlaps. Tungsten was also slightly less compressible than Mo, thus it is not as sensitive to changes in pressure as Mo. Consequently, Mo was the logical choice for use as a pressure calibrant in this experimental set-up. Ruby fluorescence would have obviously been the preferred pressure calibrant but could not be used due to the lack of appropriate spectroscopic equipment at CHESS.

3.1.4. X-ray Diffraction Experimental Errors

In addition, recall from Section 2.4 that due to the width size of the up-stream and down-stream slits, used for discriminating between different angles, there is an experimental error in the selection of the angle at which the detector was placed. For instance, if the width of the slits is 200 μm and the detector is placed at a 2θ angle of 12.0° this would result in an error of 0.150 keV Å. Incidentally the E•d (Energy x d-spacing) value at 12.0° is 59.314 keV Å. In addition, there is also an extrinsic error in

the ability of the Ge detector to discriminate between different energies. The detector resolution worsens with the square root of the energy.

Along with these two previously mentioned errors, there have been other errors discovered during the course of the experiments. It was noticed that the correct replacement of the DAC into the beam line was critical, in order to maintain the same E•d value. A change of 200 μm along the z-axis, (along the beam) would result in a 0.300 Å keV change in the value of the E•d. Consequently, some scatter in the data is expected, simply due to these experimental errors.

§3.2: CuO X-ray Diffraction Results

As previously mentioned, the samples of CuO were studied under various conditions. Table 3.1 lists these conditions.

Table 3.1: The experimental conditions of each experimental CuO run accomplished at the CHESS facility.

Experiment Date	Run Name	Medium	Pressure Gauge	Maximum Pressure
Sept. 1992	LP2	M:E	Gasket/Ruby	N/A
May 1993	LP3	None	Mo	25 GPa
Aug. 1993	LP4	Silicone Oil	Mo	25 GPa
Oct. 1993	HP5	None	Mo	60 GPa

The samples of CuO were studied using the energy dispersive X-ray diffraction (EDXD) technique at the CHESS facility at Cornell University in Ithaca N.Y. Figure 3.5 shows a typical X-ray diffraction pattern of CuO mixed with a pressure calibrant of Mo. Thirteen distinct CuO peaks were visible in the energy range shown in Figure 3.5. In one spectra, a total of 29 CuO peaks (the maximum number of peaks seen in any spectrum) are visible over an energy range of 15-90 keV and are listed in Table 3.2. The 8 peaks systematically used in the structure fits are listed in Table 3.3. To achieve consistent and reliable values for the lattice parameters, effort was made to use only and all of the peaks listed in Table 3.3. However there were cases where this was just not possible, due to peak overlap.

3.2.1 CuO Lattice Parameter Determination

One of the difficulties in attaining accurate lattice parameters was, as just mentioned, the overlap of Mo and CuO peaks throughout the entire pressure range examined. The Mo (200) and the CuO (202) peaks overlapped under room conditions and did not separate until 32 GPa was surpassed. In addition the (111) peak of CuO merged with the (110) peak of Mo at 8 GPa and they separated

at 25 GPa. This was important since the (111) peak was expected to be the most intense and the fits of the parameters were done with the area of the peak being used to give weight to the value. The last major Mo peak (211) overlapped with the CuO (22-2) peak at 25 GPa, fortunately the Mo peak was consistently greater then the CuO peaks surrounding it and thus its value could be attained with some certainty. At the same pressure of 25 GPa the Mo (200) peak separated from CuO (202). In addition there were other Mo peaks at higher energies that again were much stronger then the CuO peaks surrounding it, thus there were consistently 3 or 4 usable Mo peaks for pressure calculation.

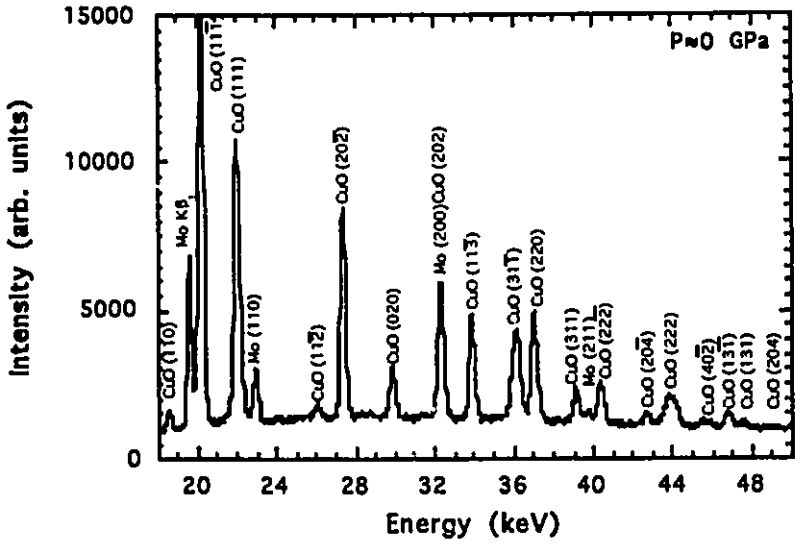

Figure 3.5 An indexed X-ray energy dispersive diffraction pattern of the CuO sample from the run HP5 at room pressure.

The peaks shown in Figure 3.5 were used in the calculation of the lattice parameters of monoclinic CuO at room pressure. These peaks and others at still higher energy are shown in Table 3.2 along with their corresponding d-spacing values. For comparison of the accuracy of the fit, the observed peak energies are shown alongside the calculated peak energies. The energies were calculated from the fitted lattice parameters for the monoclinic CuO structure: a=4.6873 Å, b=3.4290 Å, c=5.1166 Å, β=99.70° and a unit cell volume of 81.064 Å^3. The calculated energy values for the diffraction

Table 3.2: Comparison of the observed and calculated energy values of the lines fitted in the room pressure spectrum recorded during the HP5 run. The fitted lattice parameters are given in the text. Some of these lines are shown in the diffraction pattern of CuO in Figure 3.5.

(hkl)	d-spacing (Å)	Energy obs (keV)	Energy cal (keV)	difference (keV)
(110)	2.7502	18.566	18.546	0.020
(11-1)	2.5258	20.216	20.216	0.000
(111)	2.3185	22.023	22.001	0.022
(11-2)	1.9588	26.067	26.048	0.019
(20-2)	1.8655	27.371	27.345	0.026
(020)	1.7110	29.843	29.783	0.060
(202)	1.5814	32.288	32.392	-0.104
(11-3)	1.5057	33.912	33.960	-0.048
(31-1)	1.4130	36.137	36.200	-0.063
(220)	1.3781	37.052	37.087	-0.035
(311)	1.3043	39.148	39.197	-0.049
(22-2)	1.2644	40.384	40.434	-0.050
(20-4)	1.1956	42.707	42.743	-0.036
(222)	1.1632	43.897	44.001	-0.104
(40-2)	1.1220	45.509	45.417	0.092
(13-1)	1.0916	46.776	46.719	0.057
(131)	1.0739	47.547	47.519	0.028
(204)	1.0414	49.031	49.295	-0.264
(024)	1.0153	50.292	50.269	0.023
(313)	1.0067	50.721	50.819	-0.098
(22-4)	0.9807	52.066	52.097	-0.031
(420)	0.9575	53.327	53.299	0.028
(42-2)	0.9383	54.419	54.309	0.110
(33-1)	0.9204	55.477	55.538	-0.061
(331)	0.8875	57.534	57.539	-0.005
(040)	0.8572	59.567	59.563	0.004
(51-3)	0.8447	60.449	60.268	0.181
(333)	0.7743	65.945	66.007	-0.062
(315)	0.7647	66.773	66.695	0.078
(242)	0.7548	67.648	67.797	-0.149

peaks of CuO, listed in Table 3.2, are in good agreement with those observed in Figure 3.5.

Following the final CHESS run, a literature search revealed a recently released paper by Åsbrink et al. on the pressure behaviour of CuO up to 50 GPa.[10] In his paper, Åsbrink showed that allowing an hour to pass between a pressure increase and recording a diffraction spectrum could change the values of the bulk modulus B_0 by as much as 30% and the pressure derivative B_0' by 25%. The time dependence of the relaxation of the lattice was not known when the experiments were being conducted. Consequently, immediately after the pressure was increased, the DAC was placed back into the X-ray beam, without any systematic allowance for the solid to relax. However the data as shown in Figures 3.6a, b, and c are still in good agreement with the published data. The slight differences, and the reasons that they occur, will be discussed.

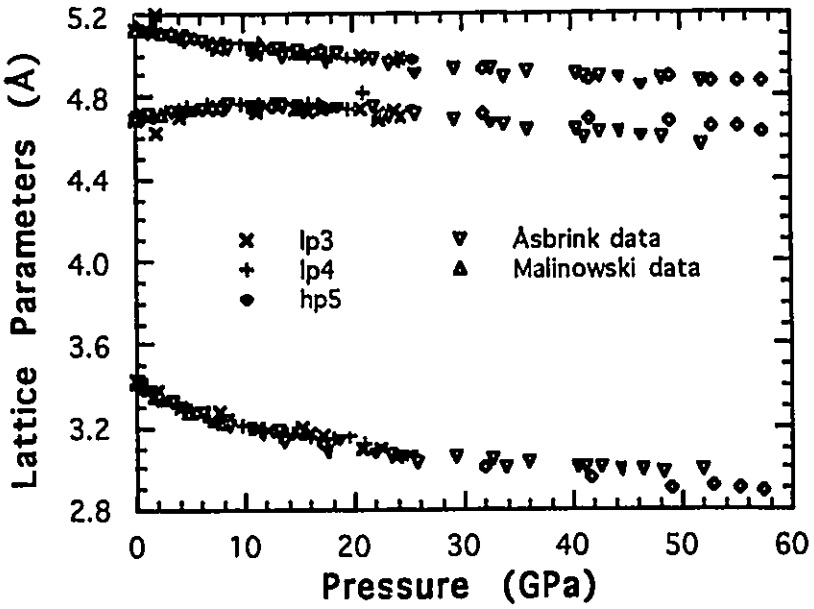

Figure 3.6a: A plot of the lattice parameters a, b, c versus pressure for data attained from the indicated chess runs in order to compare with the data obtained by two pressure research groups, Åsbrink et al.[10] and Malinowski et al.[23]

It was noticed from Figure 3.6b that there is some scatter of the β lattice parameter values. This is due to the fact that a relatively large change in β (if β≈90°) is needed to cause a

noticeable change in the unit cell volume of the structure as indicated in Figure 3.7. In contrast to the scatter in the values of β, there is relatively little scatter in the other calculated lattice parameters or the value for the volume as shown in Figures 3.6a and c.

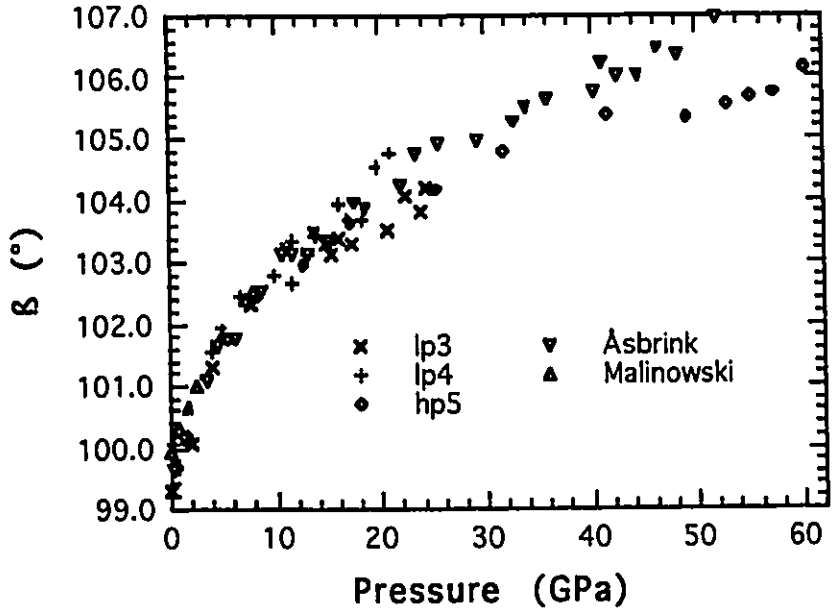

Figure 3.6b: A plot of the lattice parameters β versus pressure for data attained from the indicated CHESS runs. Data obtained by two pressure research groups, Åsbrink et al.[10] and Malinowski et al.[23] are also plotted

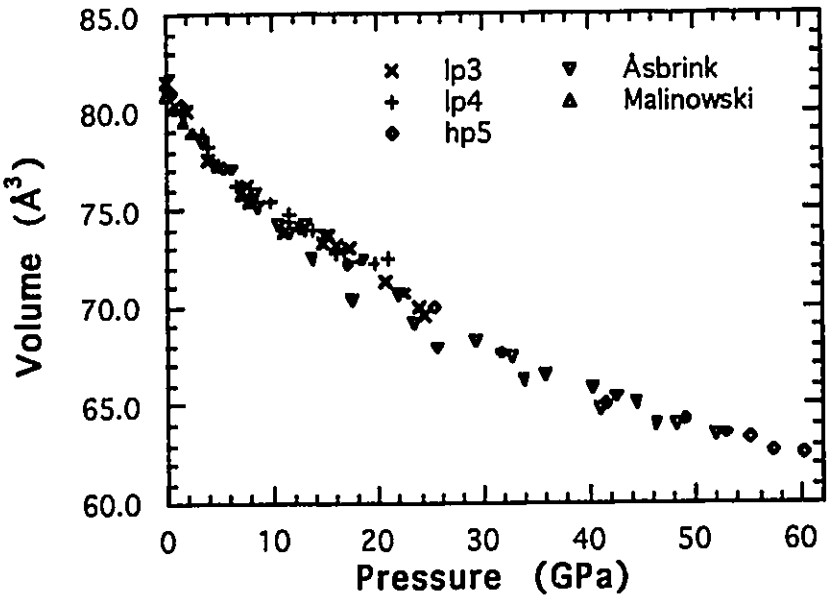

Figure 3.6c: A plot of the unit cell volume versus pressure for data attained from the indicated CHESS runs. Data obtained by two pressure research groups, Åsbrink et al.[10] and Malinowski et al.[23] are also plotted.

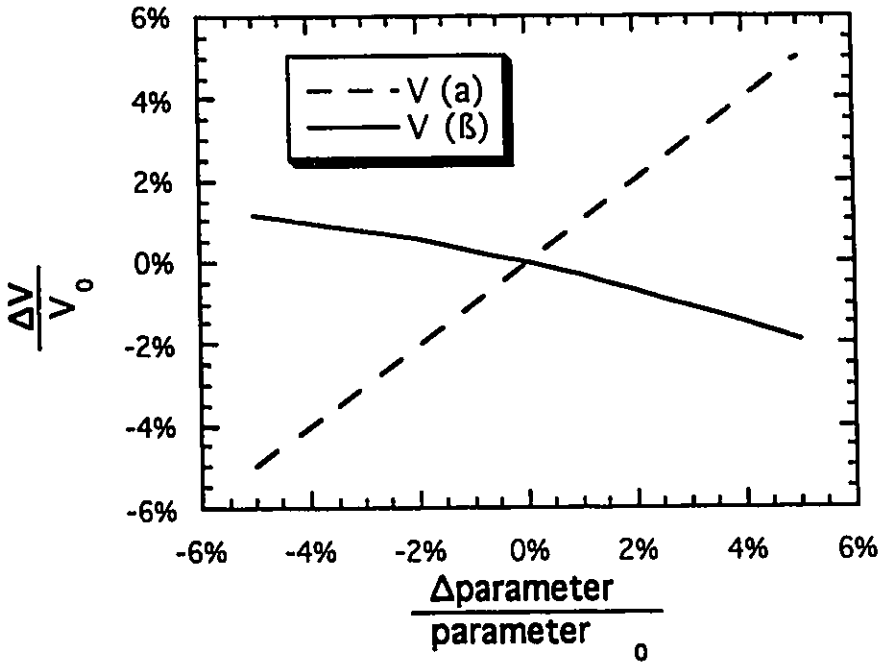

Figure 3.7: Plot of the change in volume with a change in β or the a-lattice parameter for the tenorite structure. The room condition values of CuO were used for the V_0, a_0, and β_0 values. The volume change was calculated by finding the volume by varying only the indicated parameter and then calculating the relative change in the volume.

§3.2.2 Why are the Peak Intensities Changing?

Figure 3.8 shows a series of diffraction patterns taken during the HP5 run of a sample of CuO at the indicated pressures. From this series of patterns, it can be noticed that the (200) peak at 22 keV, disappears. At 60 GPa the (110) peak should be visible in the energy range that Figure 3.8 is showing. It was noticed that the (110) peak started to increase with energy (as expected) as the pressure increased. It slowly combined with the Mo $K_{\beta 1}$ fluorescence peak, but as the pressure was continuously increased to 60 GPa, the (110) peak never reemerged, although a calculation of its d-spacing would place the (110) peak where there were no other peaks to interfere with it at higher pressure.

Although conclusions based on peak intensities are suspect due to preferred crystal orientation, the observed change in the intensities of the diffraction peaks could indicate a change in the

positions of the oxygen atoms. This result is substantiated by research done by Forsyth et al.[33] They showed that the oxygen positional parameter y had changed from 0.4207 at room pressure to 0.4022 at 2.2 GPa.

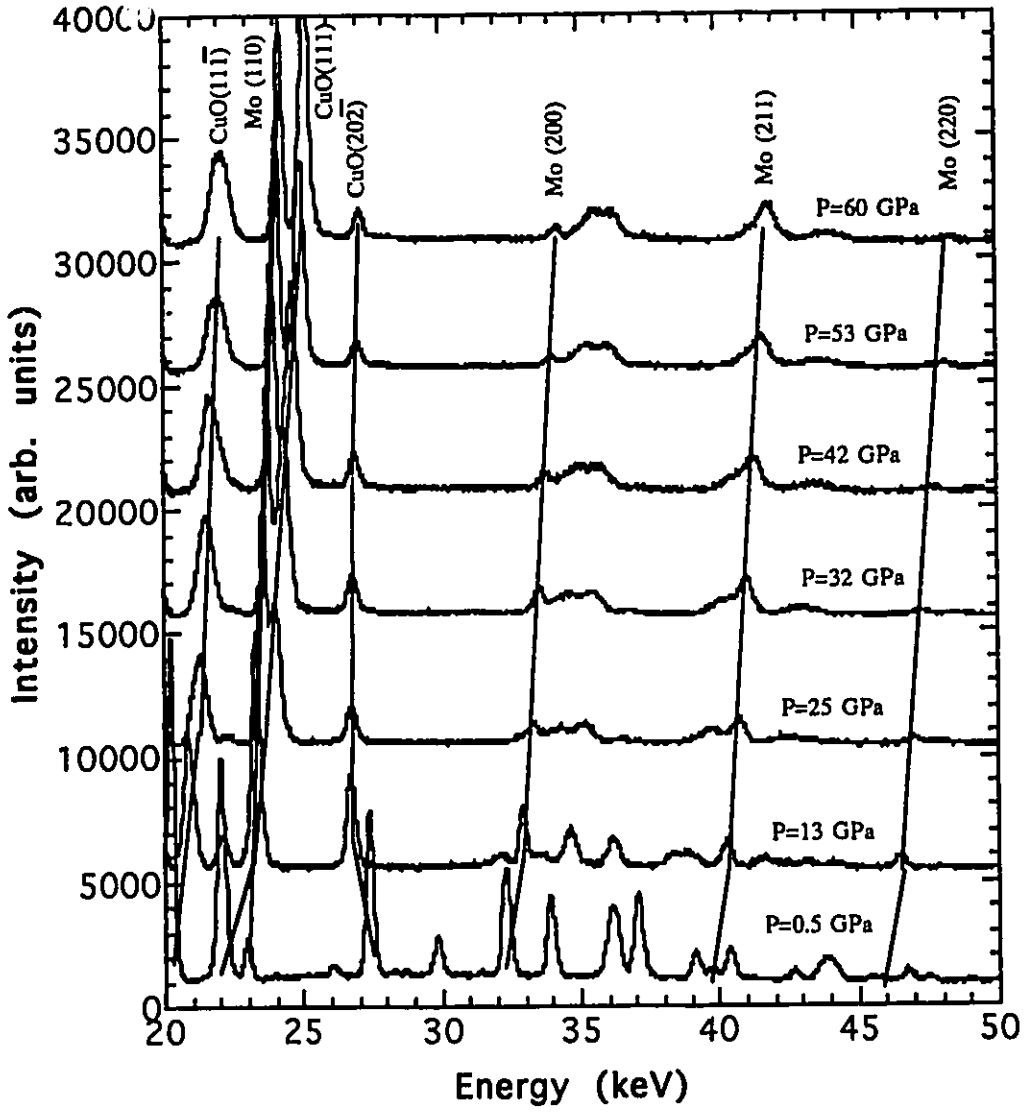

Figure 3.8: A series of X-ray diffraction spectra of a CuO sample (no pressure medium) and a Mo pressure gauge at different pressures. Also indicated in this plot is the movement of the Mo lines and some CuO lines with pressure. In addition the peak intensities were multiplied by a factor to yield the same value for the (111) CuO peak at each pressure.

The decrease in the y parameter would result in an increase in the calculated intensity of the monoclinic peak (111),

subsequently decreasing the relative intensity of the other peaks. Figure 3.9 shows a plot of the calculated peak intensities for CuO at 41.5 GPa using different values for the oxygen atom positional parameter, y. Thus if the y parameter had increased then both (11-1) and (20-2) calculated peak intensities would increase. Figures 3.8 indicates that although the observed peak intensity of (11-1) did increase relative to observed (111) with pressure, (20-2) did not. If the y parameter decreased in value then both of the calculated peak intensities for (11-1), (20-2) would have decreased in intensity and as just indicated this did not occur. Thus a change in the y parameter does not satisfactorily explain all the changes in the peak intensities as the pressure was increased.

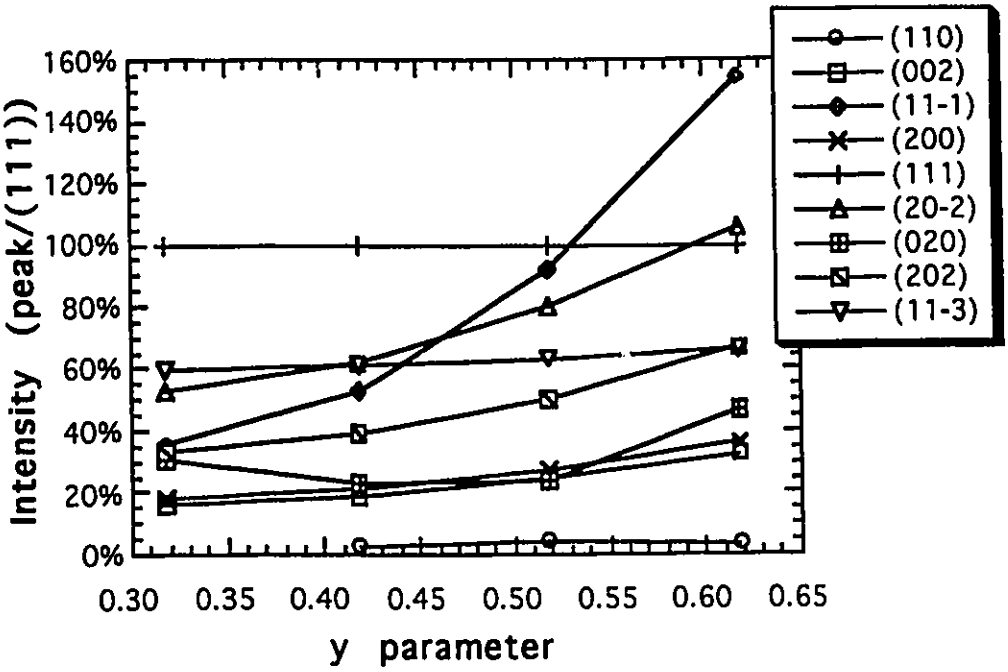

Figure 3.9: Plot of the relative intensity of the indicated diffraction peak versus y, (the oxygen atomic position parameter) normalized to the intensity of the (111) diffraction peak of CuO (space group C2/c with the atomic positions:
4 Cu atoms: (1/4,1/4,0), (3/4,1/4,1/2), (3/4,3/4,0), (1/4,3/4,1/2)
4 O atoms: (0,y,1/4), (0,-y,3/4), (1/2,1/2+y,1/4), (1/2,1/2-y,3/4)).
At room conditions y=0.4207.[33]

§3.2.3 A Careful Study of CuO to 15 GPa

Recall that a phase change at 10 GPa has been mentioned, but never confirmed. Consequently a careful analysis of CuO to 15 GPa was undertaken to investigate the possibility of such a transition.

Using all of the values shown in Table 3.3, the four lattice constants for the monoclinic structure were calculated. Figures 3.11a, b, and c show how the lattice constants change with pressure. The a-lattice parameter increases to a value of 4.75 Å at a pressure of 12 GPa at which point it starts to decrease. The b- and c-lattice parameters smoothly decrease with pressure while the β value increases with pressure.

Table 3.3: Peaks used to fit the structure and their d-spacing values near room conditions (HP5 run).

(hkl)	d-spacing (Å)
(11-1)	2.5258
(111)	2.3185
(20-2)	1.8655
(020)	1.7110
(202)	1.5814
(11-3)	1.5057
(31-1)	1.4130
(220)	1.3781
(31-3)	1.1702

At 10 GPa the sample was viewed and no change in the colour of the sample was noticed. There were also no discontinuities visible as the pressure was increased to 15 GPa in the series of plots Figure 3.11a, b, c. Figure 3.10 shows an indexed X-ray diffraction pattern of the CuO sample at 12 GPa, all the peaks were accounted for and no new peaks were visible. Thus there was no phase transition visible at 10 GPa as suspected by Malinowski,[23] Åsbrink[10] or Reimann and Syassen[15].

Earlier (Section 3.1.2) I showed that at approximately 8 GPa M:E freezes. Figures 3.2 and 3.3 show distinct changes in the ruby fluorescence spectra, most notably after the liquid-to-solid transition of the pressure medium. In addition, Figure 3.4 shows how the line broadening and the R_1-R_2 separation increases substantially as a result of the pressure medium phase transition. Thus the report of a phase transition of CuO at 12±2 GPa could be simply due to the freezing of the pressure medium and hence not due to a real phase transformation of the sample.

As shown in Figure 3.10, all of the major peaks have been satisfactorily accounted for, by either a Mo or CuO X-ray diffraction peak. The intensity (histogram) of the diffraction peaks was calculated using a routine available within the program XRDA. XRDA is capable of calculating the intensity of the diffraction lines with the following corrections taken into account: photon spectrum at the CHESS B1 beam line (previously discussed in Section 2.4), absorption of X-rays by air and diamonds, multiplicity, structure factor, atomic absorption by the sample and detector sensitivity.

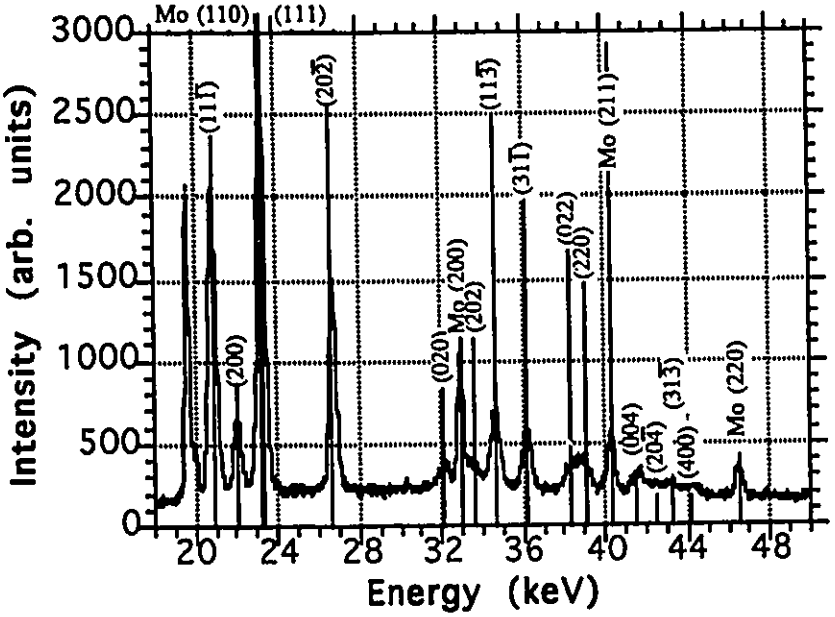

Figure 3.10: An indexed X-ray diffraction pattern at 12 GPa of monoclinic CuO (a=4.749 Å, b=3.179 Å, c=5.038 Å, and β=103.0°) and cubic Mo (a=3.102 Å) from the HP5 run. For the intensity peak calculation the room pressure atomic positions were used.

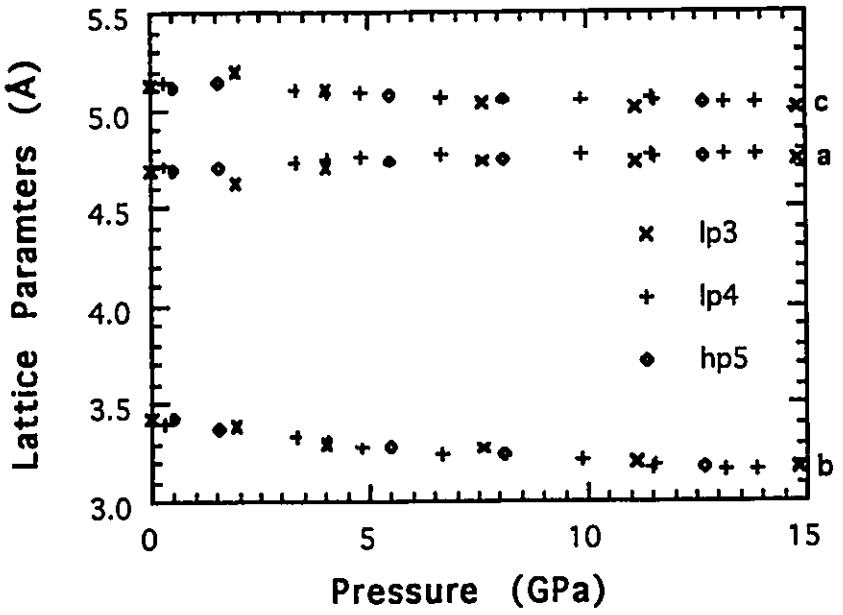

Figure 3.11a: A plot of the lattice parameters a, b, c, versus pressure for the monoclinic CuO structure up to 15 GPa.

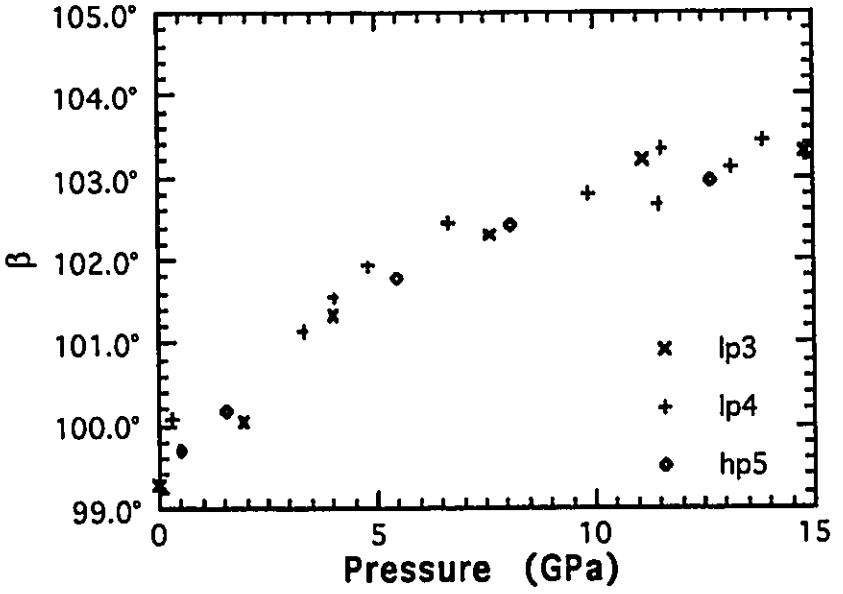

Figure 3.11b: A plot of the lattice parameter β versus pressure for the monoclinic CuO structure up to 15 GPa.

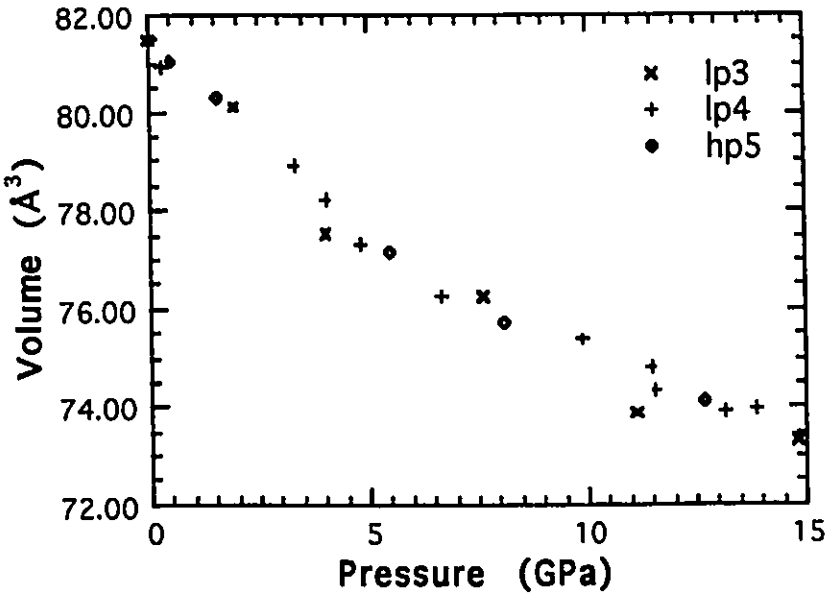

Figure 3.11c: A plot of the lattice volume versus pressure for the monoclinic CuO structure up to 15 GPa.

Table 3.4: Comparison of the observed and calculated energy values of the peaks shown in the diffraction pattern of CuO in Figure 3.10.

(hkl)	d-spacing (Å)	Energy obs. (keV)	Energy calc. (keV)	difference (keV)
(11-1)	2.4471	20.866	20.889	-0.023
(200)	2.3147	22.060	22.065	-0.005
(111)	2.1946	23.267	23.224	0.043
(20-2)	1.9113	26.716	26.715	0.001
(020)	1.5886	32.143	32.122	0.021
(202)	1.5232	33.523	33.550	-0.027
(11-3)	1.4746	34.628	34.626	0.002
(31-1)	1.4122	36.158	36.155	0.003
(022)	1.3331	38.303	38.268	0.035
(220)	1.3123	38.910	38.971	-0.061
(004)	1.2258	41.656	41.605	0.051
(20-4)	1.2021	42.477	42.495	-0.018
(31-3)	1.1818	43.207	43.170	0.037
(400)	1.1563	44.160	44.130	0.030
(22-4)	0.9614	53.112	53.268	-0.156
(13-3)	0.8918	57.257	57.116	0.141

A plot of the d-spacings of the X-ray diffraction peaks measured versus pressure is shown in Figure 3.12. Peaks (002), (200) (before it disappears) and (11-1) appear to be converging to a d-spacing of 2.4 Å, while (111) and (20-2) approach 1.95 Å, and (020), (202), (11-3), (31-1) are approaching 1.4 Å.

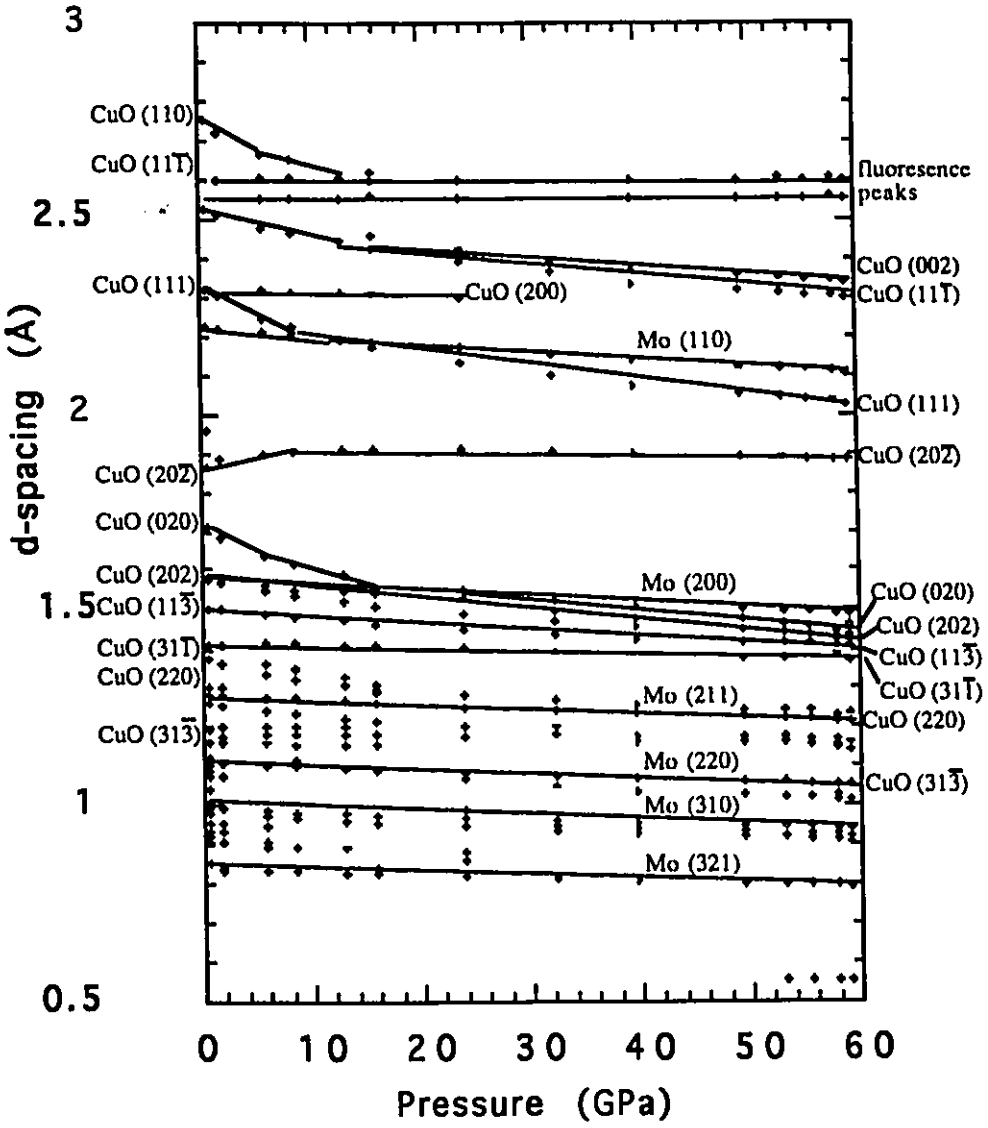

Figure 3.12: d-spacing versus pressure of the peaks fitted in the spectra of the HP5 run. The peaks used consistently for the fitting of the lattice parameters and peaks of interest of the monoclinic CuO parameters are indicated by lines drawn through the data points. In addition how the peaks change with pressure are shown.

§3.2.4 Investigation of a Possible New Structure

During the investigation of CuO to a pressure of 60 GPa, it was noticed that the peak intensities were changing and in addition or a result of this change of intensity, the number of peaks visible decreased. Recall from Section 1.4.1 the discussion on the packing fraction and how it can help in predicting what the new phase transition may be. In the case of CuO, the next phase it "should" transform to, is rocksalt. In an attempt to explain the changes seen in CuO, an investigation of a possible new structure (i.e. rocksalt) was undertaken.

The ratio between 2.4 Å and 1.95 Å, 1.4 Å is 0.813 and 0.583 respectively. Compare these two values with the ratios between the (111) and (200), (220) peaks of an ideal face-centered cubic (FCC) structure, which are 0.866 and 0.612 respectively. Figure 3.13 is a plot of the ratio of the monoclinic (11-1)/(111) d-spacing versus pressure. These plots indicate that these peaks are approaching the same value (111)/(200) d-spacing ratio for a FCC structure. There is however still a large gap separating the ratio of the monoclinic peaks with that of the cubic peaks.

Two of the points (at 2 and 42 GPa) in Figure 3.13 do not appear to follow the trend the other points have set. This is simply due to the overlap of peaks resulting in a poor fit in one or both of the peak values. If the suspected cubic (or distorted cubic) structure is valid, then the monoclinic peak (20-2) must be accounted for, since as shown in Figures 3.10, 3.12, and 3.16, it is a distinct peak, but not a peak of the suspected new structure. As mentioned earlier, the distorted rocksalt transition could be a gradual one. Thus the sample of CuO could have two coexisting crystalline phases. If this were true then the (20-2) peak should be decreasing in intensity relative to a suspected rhombohedral (distorted rocksalt) peak (200) which is equivalent in d-spacing to the monoclinic (111) peak. This relative decrease in the intensity of the (20-2) peak is shown in Figure 3.14. Although these facts are

important, they do not by themselves prove that a transition has or is occurring.

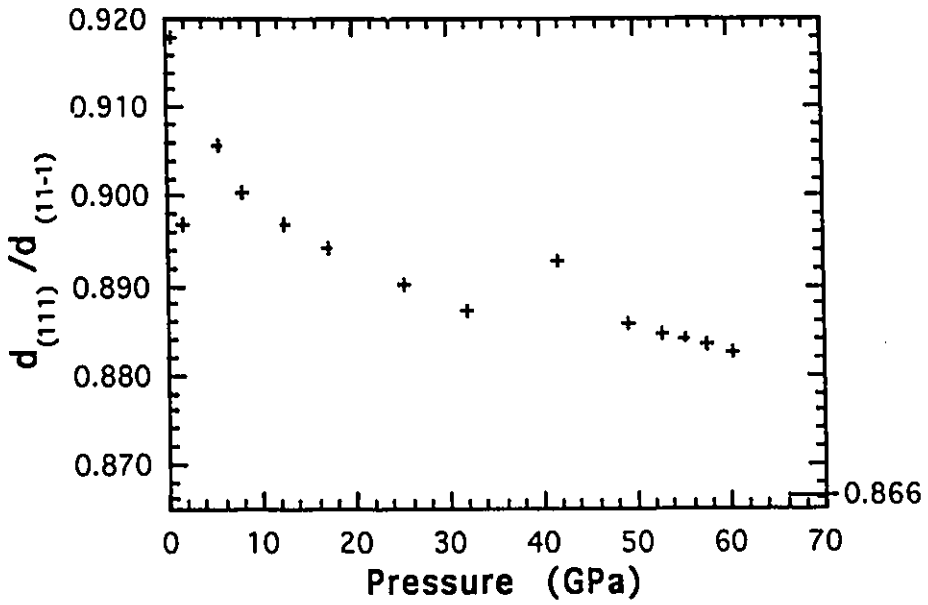

Figure 3.13: A plot of the monoclinic d(111)/d(11-1) versus pressure. For reference the d-spacing ratio for the (111)/(200) peaks of a cubic structure is shown.

Additionally Figure 3.15, a plot of the molar volume versus the cube of the anion-cation distances, shows a change of slope with pressure. It should be kept in mind that this plot is not entirely accurate because the true positions of the oxygen atoms as pressure is increased are not well known. The room condition lattice positions (see Figure 3.8) with the oxygen positional parameter y constant were used in the calculation of the anion-cation distances. It was noticed that there are two values for the anion-cation distances under room conditions, 1.957 Å and 1.954 Å, (nearest and next-nearest neighbours) the average value of 1.956 Å was used. This is the same procedure as used by Lin-Gun Liu and Bassett[7] for calculating the anion-cation distances when this situation arises.

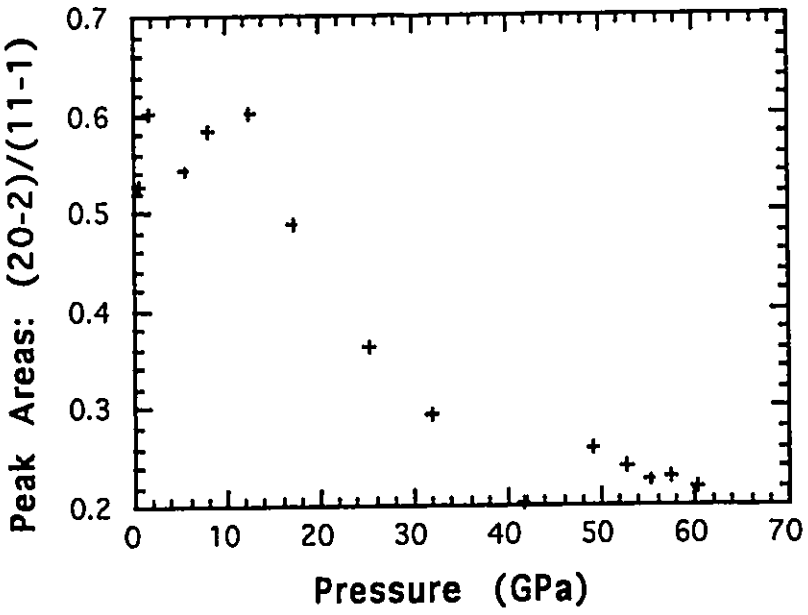

Figure 3.14: Ratio of the areas of the fitted peaks (20-2)/(11-1) versus pressure.

The packing fraction which is the ratio between the molar volume and the anion-cation distance approaches the value of 1.50 from 1.63. This calculation was performed with the idea that it could reveal which structure the CuO may transform to by comparing the packing index against those known for other oxide structures. The lattice of particular interest is the distorted rocksalt structure which two known monoclinic oxides, $LiAlO_2$ and $LiGaO_2$[7], transform to in a pressure-induced first-order phase transition.

In addition the majority of monoxides such as MgO, CaO, BaO, EuO, to name a few, form rocksalt-type structures at room conditions. The ideal rocksalt structure has a value of 1.2045 for the molar volume/cation-anion distance. The value of 1.50 although approaching this ratio of 1.2045 is still distant as shown in Figure 3.15. The MgO distorted rocksalt structure is a rhombohedral structure. This structure has the parameters **a**, **b** and **c** equivalent to one another; angles α, β, γ, also equivalent to one another, but unlike the undistorted rocksalt structure, they are not equal to 90°.

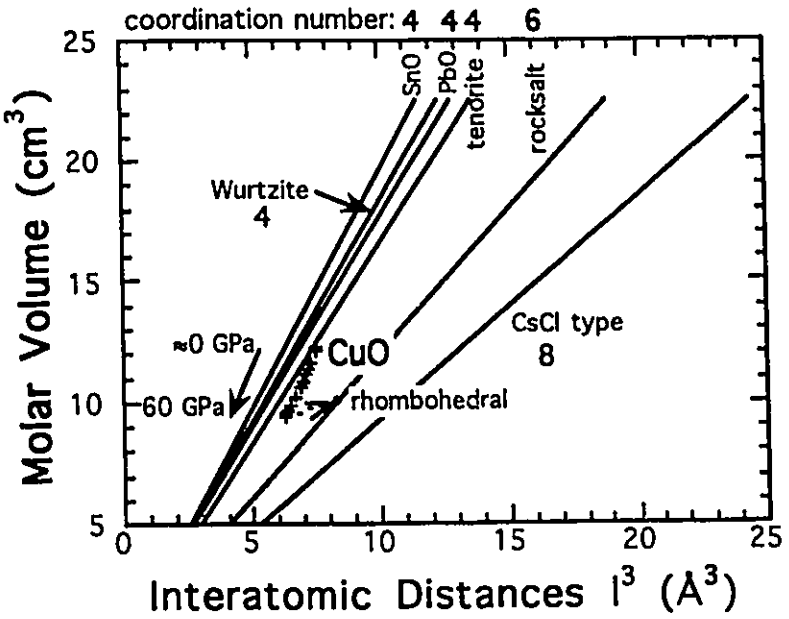

Figure 3.15: Molar volume versus the cation-anion distances of various monoxides as reported by Liu and Basset.[7] Overlaid is a plot of the change in molar volume and cation-anion distances of monoclinic CuO, indicated by (+), with pressure from experimental results and a possible transformation to the rhombohedral structure. The decreasing packing fraction first discussed in Section 1.4 starts with the left most structure and decreases as one travels to the right of the plot. Note also that the packing fraction decreases with increasing coordination number.

The diffraction plot of a CuO sample at 60 GPa shown in Figure 3.16 includes an intensity histogram calculated for the distorted rocksalt structure, giving the approximate intensity values. Using the lattice constants of **a**=4.0570 Å and γ=90.34° obtained from a fit of the rhombohedral structure and the atom placements of the rocksalt structure, the values for the molar volume and anion-cation distance are calculated to be 10.05 cm^3 and 8.3468 Å^3, respectively. These values are shown in Figure 3.15.

The possibility of a first-order phase transition from a monoclinic tenorite structure to a rhombohedral distorted rocksalt structure, cannot be proven until further research is done on CuO, to a higher pressure, possibly 70 or 80 GPa. The main reservation for the transformation is due to the slight volume increase of 6.3%. Although this does casts doubt upon the prediction, a previous monoxide (PbO)[34] does show such a transformation, from the

masicott phase to a phase with a slightly larger volume. The first phase is expected to be more yielding under pressure, while the second is consequently stiffer. If the first phase of most materials EOS were continued past the pressure point at which the transformation took place it would pass through the line representing the EOS of the new phase. In the case of PbO the first phase would have a lower volume then the third phase at a pressure of 2.5 GPa. Thus there is evidence for and against the transformation and no determination of which is true can be done until further research is conducted. No other research group has published any results that proves or contradicts beyond reasonable doubt the possibility of a phase transition to a distorted rocksalt structure or any mention of such a transition.

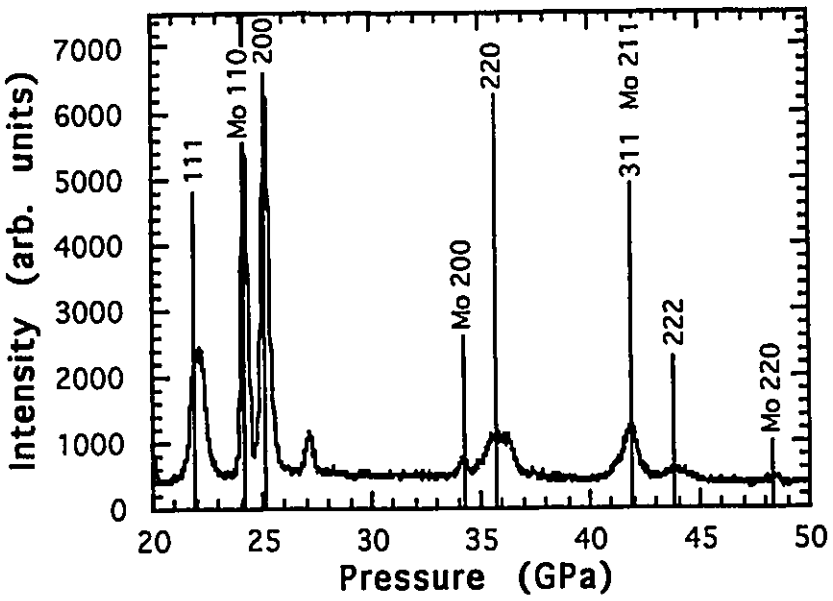

Figure 3.16: X-ray diffraction plot of a sample of CuO at 60 GPa with an overlaid histogram of the intensity values of a possible rhombohedral structure.

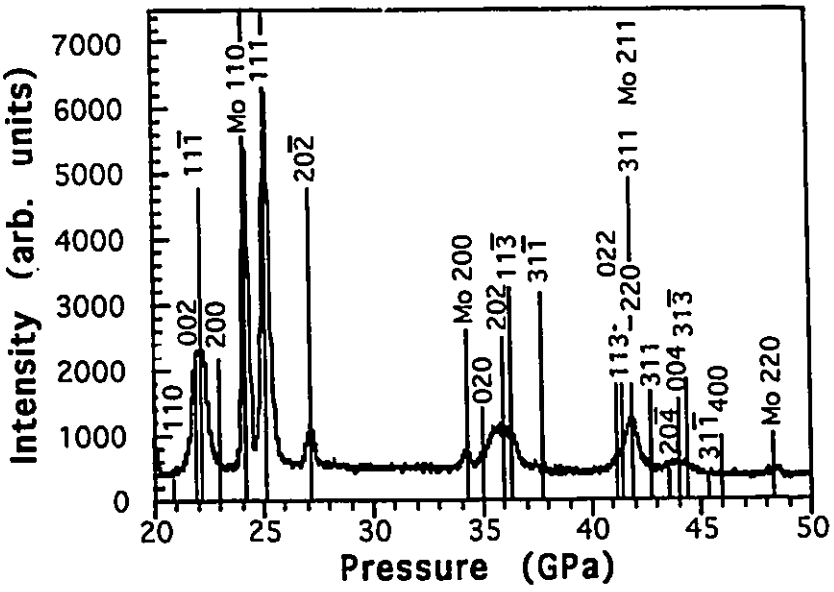

Figure 3.17: X-ray diffraction plot of a sample of CuO at 60 GPa with an overlaid histogram of the intensity values of the monoclinic structure generated by the XRDA program.[32]

Table 3.5: Comparison of the observed and calculated energy values of the peaks for a monoclinic structure, some of which are shown in the diffraction pattern of CuO (a=4.647 Å, b=2.883 Å, c=4.857 Å, β=106.2°) in Figure 3.17 at 60 GPa.

(hkl)	d-spacing (Å)	Energy obs. (keV)	Energy cal. (keV)	difference (keV)
(002)	2.3374	21.846	21.890	-0.044
(11-1)	2.2977	22.223	22.242	-0.019
(111)	2.0280	25.178	25.179	-0.001
(20-2)	1.8820	27.132	26.907	+0.225
(020)	1.4396	35.471	34.424	+0.047
(202)	1.4261	35.805	35.792	+0.013
(11-3)	1.4089	36.243	36.246	-0.003
(31-1)	1.3672	37.347	37.356	-0.009
(31-3)	1.1601	44.015	44.076	-0.061
(40-2)	1.1425	44.692	44.895	-0.203
(222)	1.0152	50.298	50.358	-0.060
(024)	0.9078	56.246	56.315	-0.069

Table 3.6 Comparison of the observed and calculated energy values of the peaks for a distorted rocksalt structure shown in the diffraction pattern of CuO (a=4.057 Å, γ=90.3°) in Figure 3.16 at 60 GPa.

(hkl)	d-spacing (Å)	Energy obs. (keV)	Energy cal. (keV)	difference (keV)
(111)	2.3374	21.846	21.934	-0.088
(200)	2.028	25.179	25.177	0.002
(220)	1.4261	35.805	35.711	0.094
(311)	1.2197	41.864	41.909	-0.045
(222)	1.1601	44.015	43.868	0.147
(400)	1.0152	50.297	50.351	-0.054

3.2.5 Comparison of Our Data with Published Results

In order to compare our data with published results, the monoclinic structure will be considered to be the only phase observable. The parameters for the third-order Birch-Murnaghan EOS, the bulk modulus, B_0, and the change of the bulk modulus with pressure at 0 GPa, B_0', were found by χ^2-minimizing routine. The fit parameters for the EOS are shown in Table 3.7 for the three CHESS runs and the data reported by Åsbrink et al.[10]

The values shown in the last column of Table 3.7 represent a fit in which B_0' was held constant at 4 and B_0 was changed in order to gain the best fit. The reason the value 4 was chosen is evident from the EOS used. Recall that the last term of the EOS:

$$\left[1+\frac{3}{4}(B_0'-4)\left\{\left(\frac{V}{V_0}\right)^{-\frac{2}{3}}-1\right\}\right]$$

which is actually only a correction for the finite strain due to pressure. By setting B_0' equal to four, the finite strain correction is negated and the remaining equation is the second-order Birch-Murnaghan EOS. The values for the fitted parameter, B_0 are relatively close to each other in value. An error value approximated from the fitted values yields a relative error of 5%. This error value

is satisfactory in light of the data used, since there was a small amount of scatter in the volume versus pressure plot. In addition the data for the three runs were taken under different conditions. The initial conditions varied in the use of different pressure medium, pressure calibrant or diamond anvil cell used. These initial conditions as demonstrated previously may slightly change the EOS of the sample. The most noticeable change is due to the pressure medium, as is evident in the data for the LP4 run (the only run to use a pressure medium). This was discussed previously in greater detail.

Table 3.7: The fitted parameters of the third order Birch-Murnaghan equation of state for the three CuO runs and the data from Åsbrink et al.[10]

CuO runs or Groups	Bulk Modulus B_0 (GPa)	Change of Bulk Modulus with pressure B_0'	B_0 with B_0'=4.0
LP3	115	4.6	119
LP4	85	12.9	125
HP5	100	6.4	131
combined	110	5.5	128
Åsbrink	93	6.7	120

In comparison to the second-order Birch-Murnaghan EOS, the fitted parameters, B_0 and B_0', for the third-order Birch-Murnaghan EOS shows a greater amount of scatter. This is expected since unlike the 2nd order EOS in which there was only one manipulated parameter, the 3rd order EOS has two parameters that are interconnected and they are adjusted to yield the best fit to the EOS.

It should also be pointed out that the runs showing the smallest values for the bulk modulus and the largest values for B_0', both used a pressure medium. Thus the slight discrepancies (i.e. lattice parameters, and EOS parameters) from the three runs are not unexpected and the results are in reasonably good agreement

with the data reported by Åsbrink et al.[10] as shown in Figure 3.16 a,b,c and Table 3.7. Recall that the results reported [23,10] were obtained with a pressure medium of methanol-ethanol (4:1) and a drilled Inconel gasket. Malinowski et al. used CaF_2 as a pressure calibrant while Åsbrink et al. used ruby fluorescence, as described in Section 2.3.1. (The EOS reported by Malinowski is not shown for the sake of clarity).

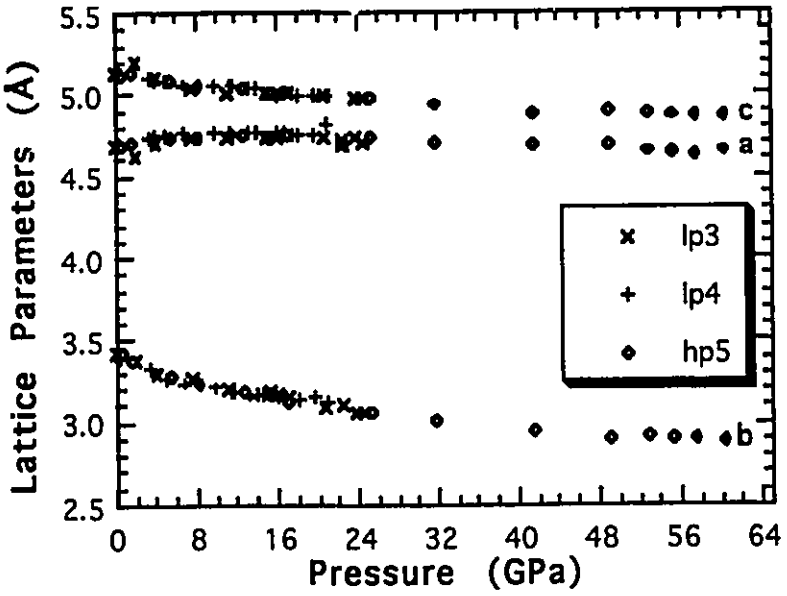

Figure 3.18:a: A plot of the lattice parameters a, b, c, versus pressure for the monoclinic CuO structure up to 60 GPa.

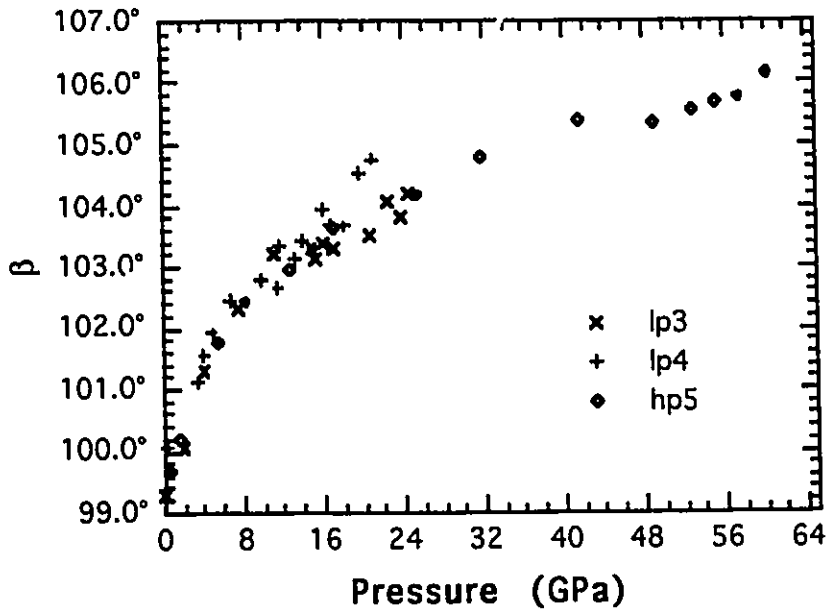

Figure 3.18:b: A plot of the lattice parameter β versus pressure for the monoclinic CuO structure up to 60 GPa.

§3.2.6 Summary of the CuO Results

In summary, there is no definite phase transition visible in CuO up to 60 GPa, the highest pressure yet attained by any research group. The plots of the lattice parameters and volume versus pressure are smooth, showing no discontinuities, which is in agreement with published results. The X-ray diffraction data shows no new peaks, but peaks that were previously observed disappeared or overlapped one another as the pressure was increased. Even though the presence of a pressure medium yields an EOS that is less "stiff" in comparison to an EOS obtained with no pressure medium, the compression results obtained with and without pressure media are comparable to those results published by other research groups.

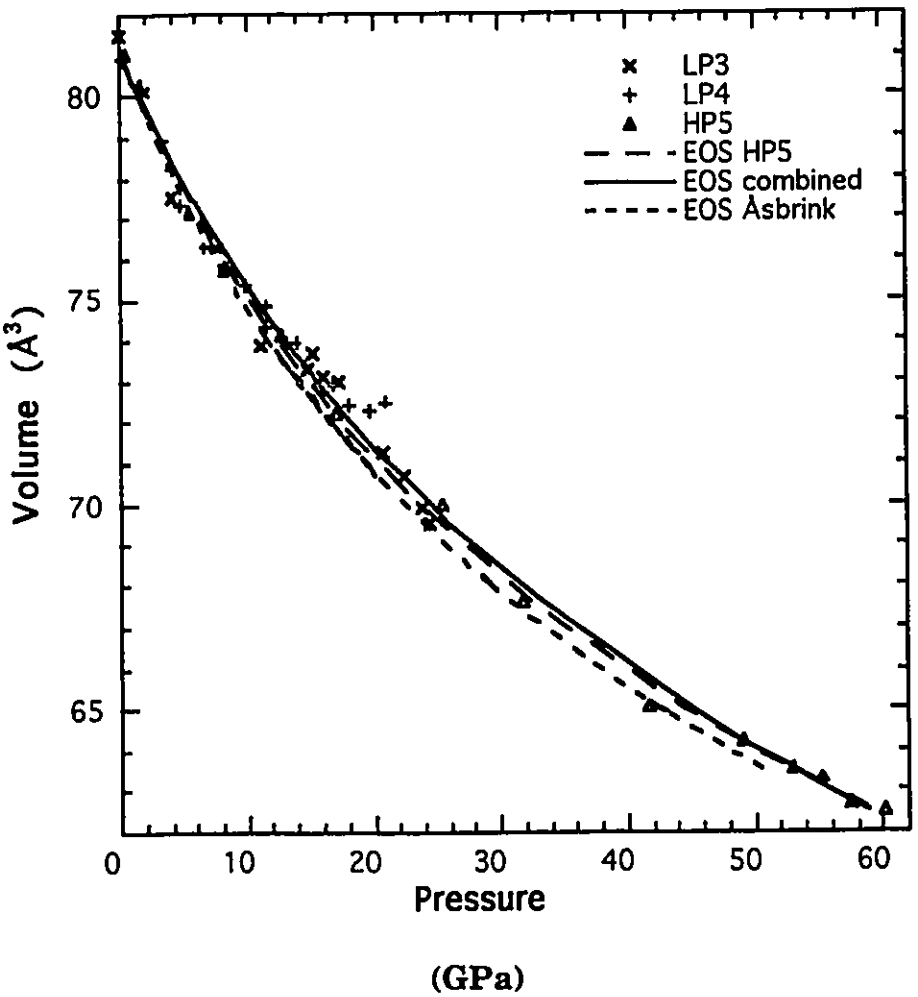

Figure 3.18:c: A plot of the lattice volume versus pressure for the monoclinic CuO structure up to 60 GPa. For comparison the third order Birch-Murnaghan EOS for the various runs are shown by the lines. (V_0=81.4 Å^3)

§ 3.3 Cu_2O Results

There were two X-ray diffraction experiments in which Cu_2O was studied. Table 3.8 lists the conditions under which each experiment was undertaken.

Table 3.8: The experimental conditions of the two Cu_2O experiments.

Experiment Date	Run Name	Medium	Pressure Gauge	Maximum Pressure
May 1993	C2HP3	None	Mo	35 GPa
Oct. 1993	C2HP5	Silicone Oil	Ruby	31 GPa

The samples of Cu_2O were studied using energy dispersive X-ray diffraction. Spectra were taken at the CHESS facility at Cornell University in Ithaca N.Y. Figure 3.19 shows a spectra of the Cu_2O at room conditions in which 12 peaks of the cubic structure are visible. These observed peaks are shown in Table 3.9, along with the calculated energy value found from the fitted lattice parameter, a=4.2358 Å. The lattice constant of Cu_2O at room conditions is 4.27 Å,[16] with 4 Cu atoms at (0.5,0.5,0.5), (0,0.5,0.5), (0.5,0,0.5), (0.5,0.5,0) and 2 oxygen atoms at (0,0,0) and (0.5,0.5,0.5). This structure can be interpreted as the Cu atoms forming a FCC structure interlaced with a BCC structure produced by the oxygen atoms. This spectrum shown in Figure 3.19 was recorded during the C2HP5 run.

The peaks listed in Table 3.10 were used to fit the lattice parameters of the various structures observed during the experiment. As previously mentioned, this will allow a systematic method for determining the lattice parameters at different pressures.

Table 3.9: Comparison of the observed and calculated energy values of the lines fitted in the near room pressure (P=0.8 GPa) spectrum recorded during the C2HP5 run. Some of these lines are shown in the diffraction pattern of Cu_2O (a=4.236 Å) in Figure 3.19.

(hkl)	d-spacing (Å)	Energy obs. (keV)	Energy calc. (keV)	difference (keV)
(110)	2.9952	17.559	17.559	-0.000
(111)	2.4515	21.454	21.506	-0.052
(200)	2.1132	24.888	24.832	0.056
(211)	1.7260	30.472	30.415	0.057
(220)	1.4992	35.081	35.119	-0.038
(311)	1.2794	41.108	41.179	-0.071
(222)	1.2230	43.004	43.013	-0.009
(400)	1.0600	49.617	49.667	-0.050
(331)	0.9726	54.076	54.121	-0.045
(420)	0.9486	55.444	55.533	-0.089
(422)	0.8652	60.788	60.827	-0.039
(511)	0.8128	64.707	64.519	0.188
(531)	0.7166	73.394	73.462	-0.068

Table 3.10: The peaks used to fit the indicated lattice structure observed for Cu_2O.

Structure	Peaks
Cubic	(111) (200) (220) (311)
Hexagonal I	(008) (103) (104) (105)[b]
Hexagonal II	(102)[a] (006) (104) (007) (108)

[a] This peak was only visible in the C2HP5 run

[b] Due to interference by other phases, consistent use of peaks was not possible for this phase in both of the CHESS runs done on a sample of Cu_2O.

Figure 3.20a and b show plots of the d-spacing values of the peaks seen in the May and October 1993 runs, respectively. The cubic structure is clearly visible in the pressure range of 0-10 GPa.

The peaks plotted between 10 and 13 GPa indicate that a phase change has occurred in the sample. Unfortunately, any information obtained in this pressure range is suspect due to the interference of a minimum of 4 different phases with one another. The possible interference may be due to BCC and HCP gasket peaks and the residual Cu_2O cubic peaks and the peaks due to the first hexagonal Cu_2O structure. There is also the possibility that some of the peaks may be due to the 2nd hexagonal phase of Cu_2O which is clearly visible above 14 GPa. Also visible above 14 GPa are the HCP gasket peaks.

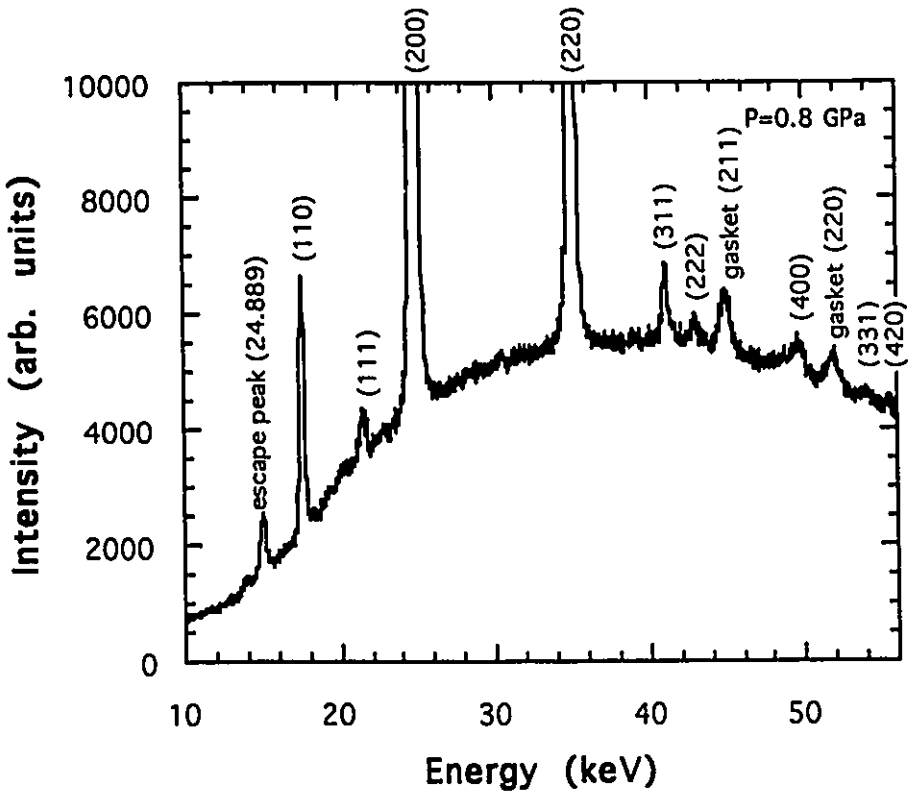

Figure 3.19: An indexed X-ray energy dispersive diffraction pattern of the Cu_2O from the C2HP5 run near room pressure. All the peaks are accounted for. Gasket lines are those of the BCC phase of stainless steel T301.

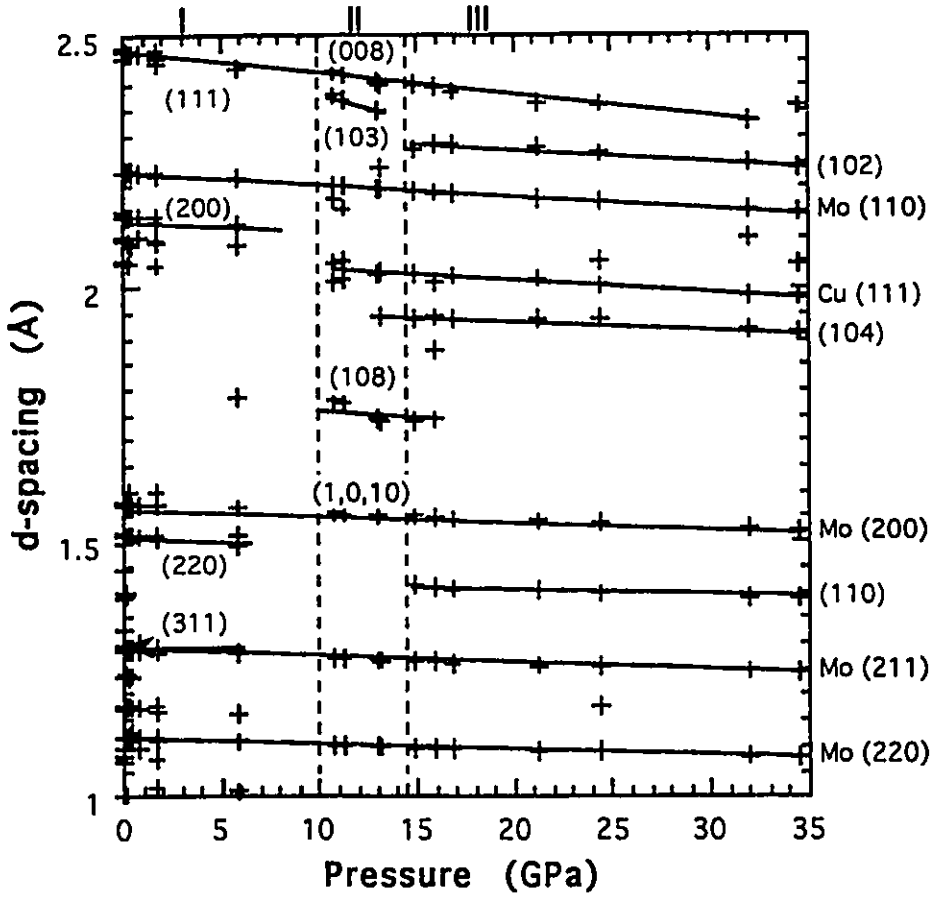

Figure 3.20a: d-spacing versus pressure showing the pressure dependence of the 3 phases of Cu_2O . Phase I is cubic, II and III are hexagonal structures for the C2HP3 run.

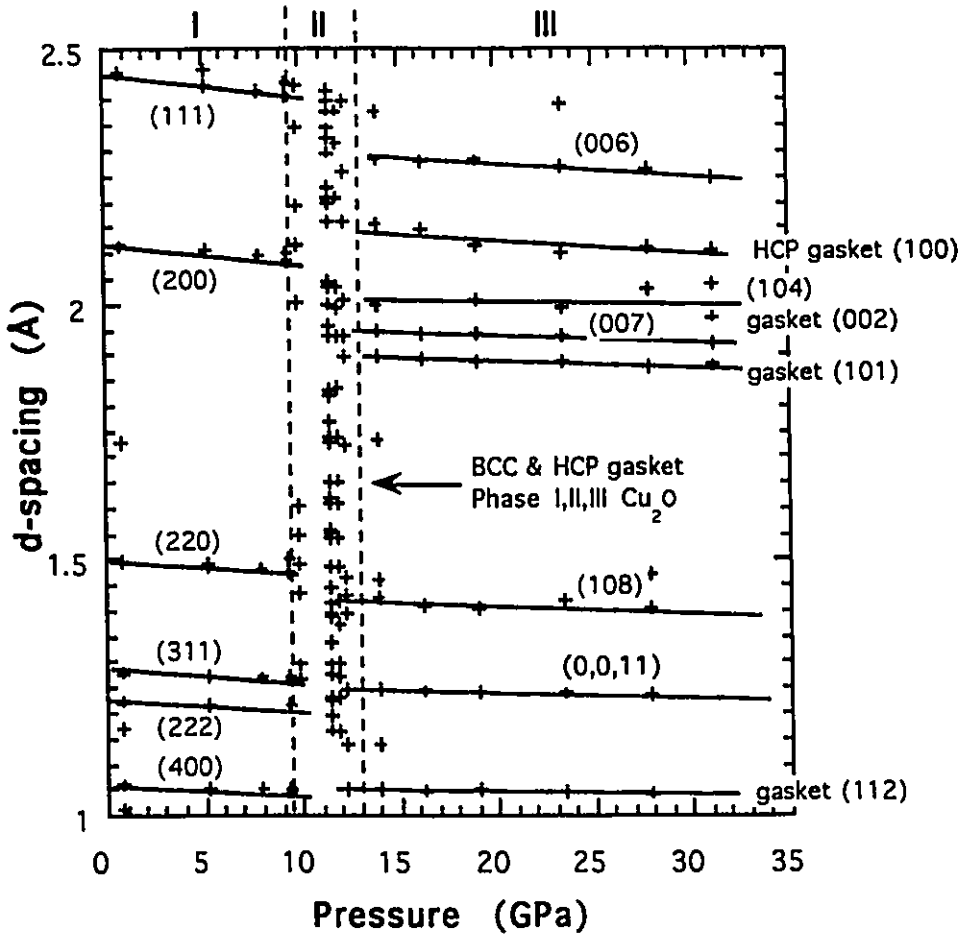

Figure 3.20b: d-spacing versus pressure showing the pressure dependence of the 3 phases of Cu_2O . Phase I is cubic, II and III are hexagonal structures for the C2HP5 run. The peak indices shown for phase III will explain all the lines observed, but are different from the indices used in Figure 3.20a.

Table 3.11: Phase transitions, structures, and lattice parameter data of the Cu_2O sample from the C2HP3 and C2HP5 runs.

pressure range (GPa)	structure type	lattice parameter C2HP3 (Å)	lattice parameter C2HP5 (Å)
≅0	Cuprite	a=4.27	a=4.24
≅10		a=4.23	a=4.20
≅10	Hexagonal	a≅2.86 c≅19.40	a≅2.88 c≅19.98
≅13		a≅2.79 c≅19.05	
16	$CdCl_2$	a= 2.82 c=12.75	a=2.84 c=12.71
at least 30		a=2.77 c=12.71	a=2.83 c=12.66

Note: for the data above, the same indices used by Werner were used to fit the data.

Table 3.12: For comparison the equivalent table of 3.11 with the results reported by Werner and Hochheimer.[16]

pressure range (GPa)	structure type	lattice parameter (Å)
0	Cuprite	a=4.27
10		a=4.18
10	Hexagonal	a=2.90 c=19.31
13		a=2.82 c=19.04
13	$CdCl_2$	a= 2.82 c=12.70
at least 24		(at 18 GPa)

The published data from Werner and Hochheimer[15] was attained with a gasketed DAC and a pressure medium of methanol:ethanol as well as silicone grease. The pressure was determined by the previously mentioned, ruby fluorescence technique (Section 2.3.1). In contrast to Werner and Hochheimer's data, the disappearance of the second phase (Hexagonal I) around 13 GPa, disagrees with their reported value of 18 GPa.

Werner and Hochheimer[16] reported that the third phase of Cu_2O could be fitted with the following peaks (102), (104), (110), and (108) with the following d-spacings: 2.275 Å, 1.935 Å, 1.405 Å, and

1.330 Å, respectively, at 23.7 GPa. This means that they fitted a two parameter function with four peaks.

Although sufficient, these peaks could also be made to fit several other hexagonal structures. It was possible to fit phase III (Hexagonal II) to a slightly different hexagonal structure using the following indexing (006), (104), (007), (108), and (0,0,11) in the C2HP5 run. The peaks, at 27.8 GPa, correspond to the following d-spacings: 2.265 Å, 2.029 Å, 1.936 Å, 1.404 Å, and 1.235 Å respectively. Table 3.11 shows the values of the d-spacing and the difference between the observed and calculated d-spacings of those reported here, and those reported by Werner.[16]

Table 3.13: The observed and calculated values for the peaks observed at 23.7 GPa for the Werner and Hochheimer[16] data and 27.8 GPa for our data (a=2.93 Å, c=13.57 Å) .

Werner and Hochheimer[15]				This work			
(hkl)	d(obs.) (Å)	d(calc) (Å)	diff. (Å)	(hkl)	d(obs.) (Å)	d(calc) (Å)	diff. (Å)
(102)	2.275	2.274	0.001	(006)	2.265	2.261	0.004
(006)	2.130	2.112	0.018	(104)	2.029	2.033	0.004
(104)	1.935	1.931	0.004	(007)	1.936	1.938	-0.002
(110)	1.405	1.407	-0.002	(110)	1.404	1.410	-0.006
(108)	1.330	1.328	0.002	(108)	1.235	1.233	0.002
(202)	1.180	1.196	-0.016				
(116)		1.171	0.009				

As can be seen from this Table 3.13, both sets of data give reasonable fits to the peaks observed. Since the number of peaks observed is small, the reliability of these fits is in question. Thus determining which is the correct fit is not possible until more data is available. However it is possible to fit the observed peaks with the Werner indexing scheme, although this will result in peaks at 2.029 Å in both runs and in the first run a peak at 2.358 Å, being left unexplained.

One explanation for the peak is that it is caused by pure copper. This peak is located where the (111) peak of Cu would appear at this pressure. No other Cu peaks were visible in the spectra to substantiate that Cu was present. It should be noted that Cu_2O at a certain pressure and temperature, see Figure 3.21, will decompose into CuO+Cu.[16] Thus the presence of Cu is a distinct possibility during pressure investigations of Cu_2O.

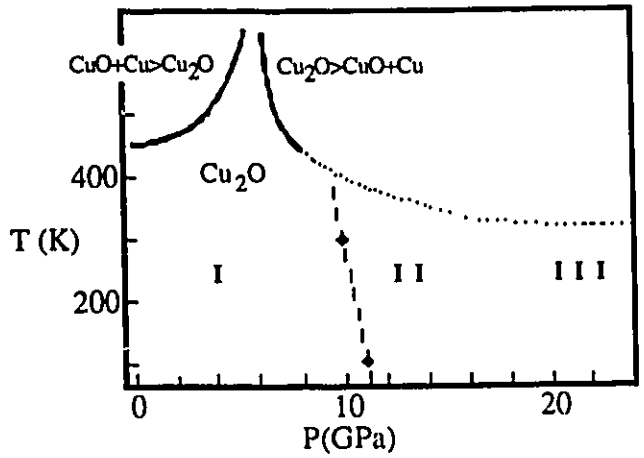

Figure 3.21: p-T diagram of Cu_2O decomposition to CuO+Cu.[16] The solid curve represents the data from Kalliomäki et al.[35]

During the C2HP3 run, Mo was used as a pressure calibrant. It was found that the interference from the Mo peaks, as is evident in Figure 3.20a, was quite severe. This resulted in poor fits of the data and precarious fits for the structure parameters. The study of Cu_2O was suspended until the ruby fluorescence method of pressure determination could be utilized at the CHESS facility.

In October 1993, the spectrometric equipment for fluorescence was made available to researchers using the CHESS facility. This allowed the continuation of the high pressure research on Cu_2O. Upon analysis of the data attained, it was noticed that gasket peaks (101), (102), (112) from the hexagonal closed pack (HCP) structure was interfering with the peaks from the Cu_2O hexagonal structures of phase II and III, due to poor X-ray beam collimation.

Figure 3.22 gives a good indication of the extent of the interference and its effect on data analysis. It is suspected that there are at least 4 if not more peaks in the 23-28 keV range. The peaks may be due to: HCP gasket (100), (002), (101) peaks, Cu_2O peaks (104) and (006) (using the Werner indexing scheme) and one peak may be due to Cu (111), the reason for suspecting Cu was previously discussed. A reliable deconvolution of this group of peaks is difficult if not impossible.

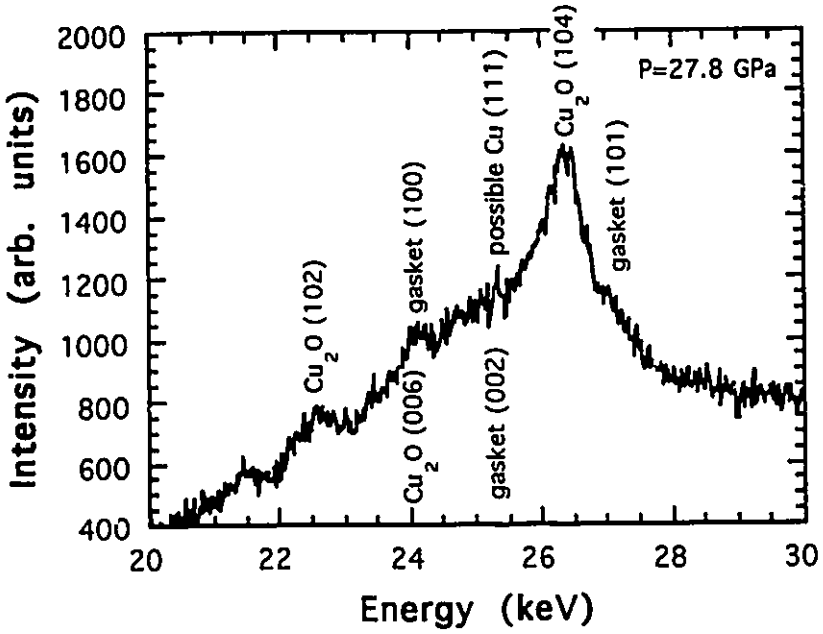

Figure 3.22: A spectrum taken at 27 GPa of Cu_2O's third phase near 24 keV which shows to what extent the interference from the gasket is affecting peak fitting. The peaks listed underneath the spectra are weak peaks and are not expected to be seen.

Although the confidence in the data analysis is not as good as one would have liked, some important observations are still possible and valid. Cu_2O at room conditions forms a cubic structure. This structure compresses smoothly until approximately 10 GPa is reached, at which point it goes through a transformation to what has been reported by Werner and Hochheimer[16] to be a hexagonal structure. It was possible to fit the hexagonal structure to the data. Unfortunately the results were too erratic due to the small number of peaks observed and interference by other structures (gasket, Mo,

Cu_2O phase I and III) to allow any further data analysis (such as calculating the EOS) to be undertaken.

Phase II (hexagonal I structure) appears to smoothly decrease with increasing pressure up to 15 GPa. At 15 GPa a second phase transition to another hexagonal structure appears. This structure also decreases smoothly with increasing pressure to 35 GPa, the maximum pressure reached. There does not appear to be a fourth phase change to this pressure. However a chemical transition due to the decomposition of Cu_2O may be occurring, evident by the possibility of the (111) Cu peak appearing in the high pressure spectra.

§ 3.4 Future Research on CuO and Cu_2O

Recall that CuO was studied to a pressure of 60 GPa. No definite phase transition was seen and the change with pressure of the volume for the monoclinic structure was smooth. However there was some discussion on the possibility that a gradual phase transition was occurring.

This idea was investigated because of the lack of peaks that were evident at the maximum pressure of 60 GPa. A prediction was made that the new structure would be distorted rock-salt. To prove or disprove this idea it will be necessary to investigate CuO well pass 60 GPa. Plans have been made to accomplish this task in the near future.

In the case of future studies of CuO there is no need for new equipment, it will be just a matter of attaining beam time at CHESS and reaching higher pressure. Unfortunately, future experiments with Cu_2O will not be as simple. It is obvious from the results reported here, that the diffraction line resolution attainable with energy dispersive X-ray diffraction is not fine enough to resolve the different phases of the sample at high pressure.

With this in mind Dr. Desgreniers has undertaken to commission the production of a low pressure DAC that uses beryllium instead of tungsten-carbide as backing plates for the diamonds. Since Be is virtually transparent to X-rays, angular dispersive X-ray diffraction (ADXD) can be accomplished. As mention in Section 2, ADXD has a much finer resolution then its counterpart, EDXD. The main drawback to the use of this cell, is that it can only attain a maximum pressure of approximately 20 GPa Fortunately this is sufficient to investigate the 3 phases of Cu_2O that have been observed in this region.

References

1 Jayaraman, A., *The diamond-anvil high-pressure cell.* Sci. Am. (USA) 250, pp. 42-51. (1984).

2 Jayaraman, A., *Diamond anvil cell and high-pressure physical investigations.* Rev. Mod. Phys. 55, pp. 65-108. (1983).

3 Raveau, B., Mervieu, M., Michel, C., Provost, J. *Recent structural developments in copper oxides high T_c superconductors.* Intern. J. of Mod. Phys. B, 1, pp. 733-44. (1987).

4 Ginzburg, V.L., *High-temperature Superconductivity.* International Journal of Modern Physics B, 1, pp. 651-680. (1987).

5 Murnaghan, F.D. Finite Deformation of an Elastic Solid. Dover, New York, (1967).

6 Poirier, Jean-Paul Introduction to the Physics of the Earth's Interior. Cambridge Univ. Press, New York, (1991). §4.3.

7 Liu, Lin-gui and Bassett, William, A., Elements, Oxides, Silicates High-Pressure Phases with Implications for the Earth's Interior. Oxford University Press, New York. (1986).

8 Liu, Lin-gun. *Structural considerations in high-pressure phase transformations of simple crystals.* High Temp.-High Press.. 13, pp. 387-98. (1981).

9 *Powder diffraction File* Card No. 5-0661. JCPDS Swarthmore, PA, USA. (1990).

10 Åsbrink, S., Gerward, L., Olsen, J. and Steenstrup, S. *High pressure studies up to 50 GPa of CuO.* High Pres. Res. 10, pp. 515-21. (1992).

11 Adams, David, Christy, Andrew, and Haines, Julian. *Second-order phase transition in PbO and SnO at high pressure: Implications for the litharge-massicot phase transformation.* Phys Rev B. 46. pp. 11358-67. (1992).

12 Hull, S and Forsyth. *The effect of hydrostatic pressure on the ambient temperature structure of CuO.* J. Phys. Condens. Matter. 3, p 5257-61. (1991).

13 Minormura, S. and Drickamer, H.G. *Effect of Pressure on the Electrical Resistance of some Transition-Metal Oxides and Sulfides.* J. Appl. Phys, 34, pp.3043-8. (1963).

14 Bourne, L. C., Yu, P. Y., Zettl, A., and Cohen, Marvin, L. *High-pressure electrical conductivity measurements in the copper oxides.* Phys. Rev. B, 40, pp. 10973-6. (1989).

15 Reimann, K. and Syassen, K. *Pressure dependence of Raman modes in CuO.* Sol. St. Comm., 76, pp. 137-40. (1990).

16 Werner, A. and Hochheimer, H.D. *High-pressure X-ray study of Cu_2O and Ag_2O.* Phys Rev B. 25, pp. 5929-34. (1991).

17 Desgreniers, S. and Legault, R. *High density crystalline Structures of copper oxides.* Proc. Int. AIRAPT. Conference AIP Conf. Proc. 309 pp. 433-6. (1993).

18 Bradley, C. C. High Pressure Methods in Solid State Research. Plenum Press, New York. (1969) Ch. 4.

19 Weir, C. E., Lippincott, E. R., Van Valkenburg, A., Bunting, E. N. *Infrared studies of the 1-15 micron region to 30,000 atmospheres.* J. Res. Natl Bur. Stand., Sec A **63**, pp. . (1959).

20 Mao, Ho-kwang and Hemley, Russell, J. *Hydrogen at high pressure.* American Scientist. **80**, pp. 234-47. (1992).

21 Lorenzana, Hector, E., Goeb, Laurent, and Jeanloz, Raymond. *Simple technique for loading hydrogen and other condensable gases in a diamond anvil cell.* Rev. Sci. Instrum. **63**, pp. 3108-11. (1992).

22 Piermanrini, G. J., Block, S. and Barnett, J. D. *Hydrostatic limits in liquids and solids to 100 kbar.* J. Appl. Phys. **44**, pp. 5377-82. (1973).

23 Malinowski, M., Åsbrink, S. and Kvick, Å. *A high-pressure single-crystal X-ray diffraction study of copper oxide using synchrotron radiation.* High Pres. Res. **4**, pp. 429-431. (1990).

24 Mao, H.K., et al. *Callibration of the Ruby Pressure Gauge to 800 kbar Under Quasi-hydrostatic Conditions.* J. of Geophys. Res. **29**, pp. 4673-6. (1986).

25 Vohra, Yogesh, K. and Ruoff, Arthur L. *Static compression of metals Mo, Pb and Pt to 272 GPa: Comparison with shock data.* Phys. Rev. **42**, pp. 8651-4. (1990).

26 Desgreniers, S. unpublished results. (1993).

27 Kinslow, Ray. ed. High-Velocity Impact Phenomena. Academic Press, New York, (1970).

28 Pearsons, W.B. Handbook of Lattice Spacing and Structures of Metals Volume 2. Pergamon Press. Toronto, (1967).

29 Margaritondo, G. Introduction to Synchrotron Radiation. Oxford University Press, New York, (1988). Chapter 2.

30 Bish, D. L., Post, J.E. ed. Modern Powder Diffraction Vol. 20. The Mineralogical Society of America, Washington D.C., (1989). pp. 326.

31 Weast, Robert, C. ed. CRC Handbook of Chemistry and Physics. 70th edition CRC Press, Inc. Boca Raton, Florida, (1990).

32 Desgreniers, S. and Lagarec, K. *XRDA: A program for energy dispersive X-ray diffraction analysis on the PC.* J. Appl. Cryst. **27**, pp. 432. (1994).

33 Fortsyth, J.B. and Hull, S. *The effect of hydrostatic pressure on the ambient temperature structure of CuO.* J. Phys.: Condens. Matt. **3**, pp. 5527-61. (1991)

34 Adams, David. et al. *Second-order phase transition in PbO and SnO at high pressure: Implications for the litharge-massicot phase transformation.* Phys. Rev. B. **46**, pp. 11358-67. (1992).

35 Kalliomäki, M. Meisalo, V, and Laisaar, A. *High pressure transformations in cuprous oxide.* Phys. Status Solidi, **56**, pp. K127-31. (1979).